THE JOURNAL OF PHYSICAL CHEMISTRY A

Article

Cite This: J. Phys. Chem. A 2019, 123, 6056−6079

pubs.acs.org/JPCA

Unified Efficient Thermostat Scheme for the Canonical Ensemble with Holonomic or Isokinetic Constraints via Molecular Dynamics

Published as part of The Journal of Physical Chemistry virtual special issue "Young Scientists".

Zhijun Zhang,[⊥,†] Xinzijian Liu,[⊥,†] Kangyu Yan,[†] Mark E. Tuckerman,[‡,§,∥] and Jian Liu[*,†]

[†]Beijing National Laboratory for Molecular Sciences, Institute of Theoretical and Computational Chemistry, College of Chemistry and Molecular Engineering, Peking University, Beijing 100871, China

[‡]Department of Chemistry, New York University, New York, New York 10003, United States

[§]Courant Institute of Mathematical Sciences, New York University, New York, New York 10012, United States

[∥]NYU-ECNU Center for Computational Chemistry at NYU Shanghai, 3663 Zhongshan Road North, Shanghai 200062, China

Supporting Information

ABSTRACT: We have recently proposed a new unified theoretical scheme (the "middle" scheme) for thermostat algorithms for efficient and accurate configurational sampling of the canonical ensemble. In this paper, we extend the "middle" scheme to molecular dynamics algorithms for configurational sampling in systems subject to constraints. Holonomic constraints and isokinetic constraints are used for demonstration. Numerical examples indicate that the "middle" scheme presents a promising approach to calculate configuration-dependent thermodynamic properties and their thermal fluctuations.

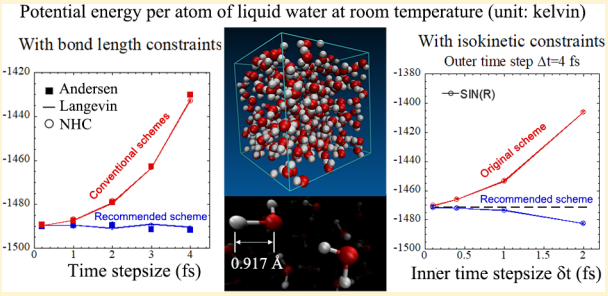

1. INTRODUCTION

Since the pioneering work by Fermi, Pasta, and Ulam in 1955[1] and that by Alder and Wainwright in 1957,[2] molecular dynamics (MD) has become a powerful and widely used tool for studying classical thermodynamic and dynamic properties of systems in chemistry, biology, and materials science.[3,4] When MD is used to perform imaginary time path integral (PIMD), it offers an efficient approach for studying quantum statistical effects in general realistic molecular systems.[5−10,87] Many cases of interest involve sampling the canonical ensemble, where the number of articles (N), volume (V), and temperature (T) are constant.

We have recently proposed a unified theoretical framework[10,11] to include various thermostat algorithms for MD[3,12−26] and those for PIMD[8,27−33] proposed in the literature for the canonical (NVT) ensemble, regardless of whether the thermostat is stochastic or deterministic. While most conventional algorithms[3,12−21,27−30,32,33] can be unified in the "side" or "end" scheme in the unified theoretical framework, the "middle" scheme suggested in refs 10 and 11 leads to more efficient and accurate configurational (i.e., conformational) sampling, irrespective of whether the thermostat is stochastic or deterministic. The "middle" scheme includes the latest progress in developing efficient Langevin thermostat algorithms[22−24,26,34] as well as provides a scenario for rationally designing various other types of efficient thermostat algorithms.[8,10,11,35]

In this paper, we generalize the unified thermostat framework to deal with systems subject to constraints. Two types of constraints are demonstrated as examples. One is the holonomic constraint that is often employed to ameliorate time-scale problems in MD simulations. The holonomic constraint is used to fix certain geometric parameters, such as bond lengths, bend angles, and torsion angles at specific values, thereby avoiding high-frequency motions. The equations of motion for a system with these geometric constraints can be numerically solved using Lagrange multipliers or projection methods. Ryckaert et al. developed the SHAKE algorithm to solve the nonlinear equations (for Lagrange multipliers) iteratively to satisfy given numerical tolerance.[36] Andersen further proposed the RATTLE variant of the SHAKE algorithm for MD using the velocity−Verlet integrator.[37] The SETTLE algorithm analytically solves the set of nonlinear equations for triatomic molecular systems.[38] Though it cannot be extended to systems with more atoms, it is very useful for constraining water molecules, which is important in biological simulations. There are various methods derived from SHAKE, such as the M-SHAKE,[39] SHAPE,[40] and LINCS[41] algorithms, which may be faster than SHAKE under certain conditions. In the present paper, we employ the SHAKE/RATTLE algorithms as examples for the component-wise solution of the undetermined Lagrange multipliers (see section S1 in the Supporting Information), but they can be directly replaced by other ones for holonomic constraints.

Received: March 24, 2019
Revised: May 21, 2019
Published: May 22, 2019

DOI: 10.1021/acs.jpca.9b02771
J. Phys. Chem. A 2019, 123, 6056−6079

The other useful constraint is the isokinetic constraint, a nonholomonic condition on the kinetic energy, used in some thermostat algorithms for systems at constant temperature. Isokinetic ensemble techniques have been proposed and formulated since the 1980s.[42−45] More recently, multiple time-step (MTS) algorithms using the Nosé−Hoover chain (NHC) approach and the isokinetic constraint have been developed.[46−49] All these algorithms, irrespective of whether the (related) equations of motion are deterministic or stochastic, implement the isokinetic constraint to restrict the kinetic energy thereby moderating the resonance effect that occurs in other MTS algorithms. We use the latest algorithm—the so-called "Stochastic-Iso-NHC-RESPA" (SIN(R))[49]—as an example to show that the "middle" scheme can lead to more efficient algorithms for SIN(R).

The paper is organized as follows. Section 2 first briefly reviews the unified thermostat framework recently developed for the *NVT* ensemble as well as the SHAKE/RATTLE algorithms for the *NVE* ensemble subject to holonomic constraints, and then it presents both conventional and novel algorithms for three typical thermostats for the *NVT* ensemble with holonomic constraints. Numerical simulations for holonomic constraints are demonstrated in section 3. Section 4 briefly reviews the SIN(R) algorithm and then proposes the new version in the "middle" scheme, followed by numerical examples in section 5. Concluding remarks are presented in section 6.

2. THEORY FOR MOLECULAR DYNAMICS WITH HOLONOMIC CONSTRAINTS

Consider a classical system with the (time-independent) Hamiltonian, which we assume to be of standard Cartesian form

$$\mathrm{H}(\mathbf{x}, \mathbf{p}) = \frac{1}{2}\mathbf{p}^T\mathbf{M}^{-1}\mathbf{p} + U(\mathbf{x}) \tag{1}$$

where $\mathbf{M}$ is the diagonal "mass matrix" with elements $\{m_j\}$ and $\mathbf{p}$ and $\mathbf{x}$ are the momentum and position vectors, respectively. The total number of degrees of freedom of the system is $3N$; therefore, $\mathbf{x}$ and $\mathbf{p}$ are $3N$-dimensional vectors, and $\beta = 1/k_BT$ is the inverse temperature throughout the paper.

2.1. Unified Framework for Molecular Dynamics in the *NVT* Ensemble without Holonomic Constraints. We first consider two prevailing MD algorithms for the *NVE* ensemble. The leapfrog algorithm for propagating a trajectory of an *NVE* ensemble through a time interval Δt is

$$\mathbf{p}\left(\frac{\Delta t}{2}\right) \leftarrow \mathbf{p}\left(-\frac{\Delta t}{2}\right) - \frac{\partial U}{\partial \mathbf{x}(0)}\Delta t \tag{2}$$

$$\mathbf{x}(\Delta t) \leftarrow \mathbf{x}(0) + \mathbf{M}^{-1}\mathbf{p}\left(\frac{\Delta t}{2}\right)\Delta t \tag{3}$$

The Kolmogorov operators relevant to the evolution are

$$\mathcal{L}_{\mathbf{x}}\rho = -\mathbf{p}^T\mathbf{M}^{-1}\frac{\partial \rho}{\partial \mathbf{x}} \tag{4}$$

$$\mathcal{L}_{\mathbf{p}}\rho = \frac{\partial U}{\partial \mathbf{x}}\frac{\partial \rho}{\partial \mathbf{p}} \tag{5}$$

The evolution operator through a time interval Δt for the leapfrog algorithm is then

$$e^{\mathcal{L}\Delta t} \approx e^{\mathcal{L}_{\mathbf{x}}\Delta t}e^{\mathcal{L}_{\mathbf{p}}\Delta t} \tag{6}$$

and is applied starting with the initial conditions $(\mathbf{x}(0), \mathbf{p}(-\Delta t/2))$. For the sake of convenience, the numerical procedure for eqs 2 and 3 for the leapfrog algorithm is denoted "x-p", in which the operations are in a right-to-left sequence by following the convention established in the recent work on the Langevin equation.[34] Similarly the velocity−Verlet algorithm reads

$$\mathbf{p}\left(\frac{\Delta t}{2}\right) \leftarrow \mathbf{p}(0) - \frac{\partial U}{\partial \mathbf{x}(0)}\frac{\Delta t}{2} \tag{7}$$

$$\mathbf{x}(\Delta t) \leftarrow \mathbf{x}(0) + \mathbf{M}^{-1}\mathbf{p}\left(\frac{\Delta t}{2}\right)\Delta t \tag{8}$$

$$\mathbf{p}(\Delta t) \leftarrow \mathbf{p}\left(\frac{\Delta t}{2}\right) - \frac{\partial U}{\partial \mathbf{x}(\Delta t)}\frac{\Delta t}{2} \tag{9}$$

which is denoted "p-x-p" with the operations in a right-to-left sequence. The evolution operator through a time interval Δt for the velocity−Verlet algorithm is then

$$e^{\mathcal{L}\Delta t} \approx e^{\mathcal{L}_{\mathbf{p}}\Delta t/2}e^{\mathcal{L}_{\mathbf{x}}\Delta t}e^{\mathcal{L}_{\mathbf{p}}\Delta t/2} \tag{10}$$

In the unified theoretical framework that we have recently proposed, most conventional thermostat algorithms[3,7,16−21,33] for the *NVT* ensemble (for the system with no holonomic constraints) can be included into either the velocity−Verlet version of the "side" scheme

$$\begin{aligned}
&\text{thermostat for half a time step } \frac{\Delta t}{2}\\
&\quad\text{(in which } \mathbf{p}(0) \text{ is updated)}\\
&\mathbf{p}\left(\frac{\Delta t}{2}\right) \leftarrow \mathbf{p}(0) - \frac{\partial U}{\partial \mathbf{x}(0)}\frac{\Delta t}{2}\\
&\mathbf{x}(\Delta t) \leftarrow \mathbf{x}(0) + \mathbf{M}^{-1}\mathbf{p}\left(\frac{\Delta t}{2}\right)\Delta t\\
&\mathbf{p}(\Delta t) \leftarrow \mathbf{p}\left(\frac{\Delta t}{2}\right) - \frac{\partial U}{\partial \mathbf{x}(\Delta t)}\frac{\Delta t}{2}\\
&\text{thermostat for half a time step } \frac{\Delta t}{2}\\
&\quad\text{(in which } \mathbf{p}(\Delta t) \text{ is updated)}
\end{aligned} \tag{11}$$

or the counterpart scheme of eq 11 which is based on the leapfrog algorithm

$$\begin{aligned}
&\mathbf{p}(0) \leftarrow \mathbf{p}\left(-\frac{\Delta t}{2}\right) - \frac{\partial U}{\partial \mathbf{x}(0)}\frac{\Delta t}{2}\\
&\textit{thermostat for a full time step } \Delta t \quad \text{(in which } \mathbf{p}(0) \text{ is updated)}\\
&\mathbf{p}\left(\frac{\Delta t}{2}\right) \leftarrow \mathbf{p}(0) - \frac{\partial U}{\partial \mathbf{x}(0)}\frac{\Delta t}{2}\\
&\mathbf{x}(\Delta t) \leftarrow \mathbf{x}(0) + \mathbf{M}^{-1}\mathbf{p}\left(\frac{\Delta t}{2}\right)\Delta t
\end{aligned} \tag{12}$$

The relevant evolution operator in the phase space for the former scheme is

$$e^{\mathcal{L}\Delta t} \approx e^{\mathcal{L}_{\mathrm{VV}}^{\mathrm{Side}}\Delta t} = e^{\mathcal{L}_T\Delta t/2}e^{\mathcal{L}_{\mathbf{p}}\Delta t/2}e^{\mathcal{L}_{\mathbf{x}}\Delta t}e^{\mathcal{L}_{\mathbf{p}}\Delta t/2}e^{\mathcal{L}_T\Delta t/2} \tag{13}$$

while that for the latter is

DOI: 10.1021/acs.jpca.9b02771
J. Phys. Chem. A 2019, 123, 6056−6079

$$e^{\mathcal{L}\Delta t} \approx e^{\mathcal{L}_{\mathrm{LF}}^{\mathrm{Side}}\Delta t} = e^{\mathcal{L}_{\mathbf{x}}\Delta t} e^{\mathcal{L}_{\mathbf{p}}\Delta t/2} e^{\mathcal{L}_{T}\Delta t} e^{\mathcal{L}_{\mathbf{p}}\Delta t/2} \tag{14}$$

In eqs 13 and 14, L_T represents the Kolmogorov operator for the thermostat. For the sake of convenience, we denote eq 11 "T-p-x-p-T" and eq 12 "x-p-T-p", where the operations are in a right-to-left sequence.

In the proposed "middle" scheme for the *NVT* ensemble (for systems without constraints),[10,11] it is suggested that

$$\mathbf{x}\left(\frac{\Delta t}{2}\right) \leftarrow \mathbf{x}(0) + \mathbf{M}^{-1}\mathbf{p}\left(\frac{\Delta t}{2}\right)\frac{\Delta t}{2}$$

thermostat for a full time step Δt (in which $\mathbf{p}\left(\frac{\Delta t}{2}\right)$ is updated)

$$\mathbf{x}(\Delta t) \leftarrow \mathbf{x}\left(\frac{\Delta t}{2}\right) + \mathbf{M}^{-1}\mathbf{p}\left(\frac{\Delta t}{2}\right)\frac{\Delta t}{2} \tag{15}$$

should be used to replace eq 3 in the leapfrog algorithm or eq 8 in the velocity−Verlet algorithm to construct efficient thermostat algorithms. That is, replace "x" by "x-T-x" for the leapfrog and velocity−Verlet algorithms (for the *NVE* ensemble), respectively. The leapfrog version of the "middle" scheme (LF-Middle)[11] reads

$$\mathbf{p}\left(\frac{\Delta t}{2}\right) \leftarrow \mathbf{p}\left(-\frac{\Delta t}{2}\right) - \frac{\partial U}{\partial \mathbf{x}(0)}\Delta t$$

$$\mathbf{x}\left(\frac{\Delta t}{2}\right) \leftarrow \mathbf{x}(0) + \mathbf{M}^{-1}\mathbf{p}\left(\frac{\Delta t}{2}\right)\frac{\Delta t}{2}$$

thermostat for a full time step Δt $\left(\text{in which } \mathbf{p}\left(\frac{\Delta t}{2}\right) \text{ is updated}\right)$

$$\mathbf{x}(\Delta t) \leftarrow \mathbf{x}\left(\frac{\Delta t}{2}\right) + \mathbf{M}^{-1}\mathbf{p}\left(\frac{\Delta t}{2}\right)\frac{\Delta t}{2} \tag{16}$$

where the relevant evolution operator in the phase space is

$$e^{\mathcal{L}\Delta t} \approx e^{\mathcal{L}_{\mathrm{LF}}^{\mathrm{Middle}}\Delta t} = e^{\mathcal{L}_{\mathbf{x}}\Delta t/2} e^{\mathcal{L}_{T}\Delta t} e^{\mathcal{L}_{\mathbf{x}}\Delta t/2} e^{\mathcal{L}_{\mathbf{p}}\Delta t} \tag{17}$$

We denote eq 16 "x-T-x-p" (LF-Middle), with the operations in a right-to-left sequence. Similarly, the velocity−Verlet version of the "middle" scheme[10] produces

$$\mathbf{p}\left(\frac{\Delta t}{2}\right) \leftarrow \mathbf{p}(0) - \frac{\partial U}{\partial \mathbf{x}(0)}\frac{\Delta t}{2}$$

$$\mathbf{x}\left(\frac{\Delta t}{2}\right) \leftarrow \mathbf{x}(0) + \mathbf{M}^{-1}\mathbf{p}\left(\frac{\Delta t}{2}\right)\frac{\Delta t}{2}$$

thermostat for a full time step Δt

$\left(\text{in which } \mathbf{p}\left(\frac{\Delta t}{2}\right) \text{ is updated}\right)$

$$\mathbf{x}(\Delta t) \leftarrow \mathbf{x}\left(\frac{\Delta t}{2}\right) + \mathbf{M}^{-1}\mathbf{p}\left(\frac{\Delta t}{2}\right)\frac{\Delta t}{2}$$

$$\mathbf{p}(\Delta t) \leftarrow \mathbf{p}\left(\frac{\Delta t}{2}\right) - \frac{\partial U}{\partial \mathbf{x}(\Delta t)}\frac{\Delta t}{2} \tag{18}$$

where the relevant evolution operator is

$$e^{\mathcal{L}\Delta t} \approx e^{\mathcal{L}_{\mathrm{VV}}^{\mathrm{Middle}}\Delta t} = e^{\mathcal{L}_{\mathbf{p}}\Delta t/2} e^{\mathcal{L}_{\mathbf{x}}\Delta t/2} e^{\mathcal{L}_{T}\Delta t} e^{\mathcal{L}_{\mathbf{x}}\Delta t/2} e^{\mathcal{L}_{\mathbf{p}}\Delta t/2} \tag{19}$$

We denote eq 18 "p-x-T-x-p" (VV-Middle).

Consider the harmonic limit where the potential energy function of the Hamiltonian eq 1 is

$$U(\mathbf{x}) = (\mathbf{x} - \mathbf{x}_{eq})^T \mathbf{A}(\mathbf{x} - \mathbf{x}_{eq})/2 \tag{20}$$

As long as the thermostat process leaves the Maxwell momentum distribution unchanged, i.e.

$$e^{L_T\Delta t} \exp\left\{-\beta\left[\frac{1}{2}\mathbf{p}^T\mathbf{M}^{-1}\mathbf{p}\right]\right\} = \exp\left\{-\beta\left[\frac{1}{2}\mathbf{p}^T\mathbf{M}^{-1}\mathbf{p}\right]\right\} \tag{21}$$

it is straightforward to follow refs 8, 10, 11, 34, and 35 to prove that the marginal distribution of the position (i.e., configuration) of the stationary state for the velocity−Verlet version of the "side" scheme (eq 11) is the same as that for its leapfrog based counterpart (eq 12), i.e.

$$\rho_{\mathbf{x}}^{\mathrm{Side}} = \frac{1}{Z_N}\exp\left[-\beta\left(\frac{1}{2}(\mathbf{x} - \mathbf{x}_{eq})^T\left(\mathbf{1} - \mathbf{A}\mathbf{M}^{-1}\frac{\Delta t^2}{4}\right)\mathbf{A}(\mathbf{x} - \mathbf{x}_{eq})\right)\right] \tag{22}$$

while that for the "middle" scheme)either "LF-Middle" eq 16 or "VV-Middle" eq 18) is

$$\rho_{\mathbf{x}}^{\mathrm{Middle}} = \frac{1}{\bar{Z}_N}\exp\left[-\beta\left(\frac{1}{2}(\mathbf{x} - \mathbf{x}_{eq})^T\mathbf{A}(\mathbf{x} - \mathbf{x}_{eq})\right)\right] \tag{23}$$

where Z_N and $\bar{Z}_N$ are the normalization constants. Note that "LF-Middle" and "VV-Middle" lead to the exact marginal distribution of configuration in the harmonic limit.[8,10,11,34,35] It is easy to prove that for *any* system, "LF-Middle" and "VV-Middle" lead to the same marginal distribution of configuration, while the former produces a more accurate marginal distribution of momentum.[11] The thermostat algorithms in the "middle" scheme are always more accurate and efficient than those conventional ones in sampling configurational space for general molecular systems.[8,10,11,34,35]

2.2. Molecular Dynamics for the *NVE* Ensemble with Holonomic Constraints. When the system is subject to the holonomic constraint

$$\boldsymbol{\sigma}(\mathbf{x}) = 0 \tag{24}$$

where $\sigma(\mathbf{x})$ is an n_c-dimensional vector as a function of the position vector $\mathbf{x}$, the time derivative of eq 24 implies the following constraint for the momentum vector $\mathbf{p}$

$$\frac{\mathrm{d}}{\mathrm{d}t}\boldsymbol{\sigma}(\mathbf{x}) = \left(\frac{\partial \boldsymbol{\sigma}}{\partial \mathbf{x}}\right)^T \mathbf{M}^{-1}\mathbf{p} = 0 \tag{25}$$

The SHAKE[36] and RATTLE[37] algorithms are two prevailing approaches for solving the discretized equations of motion of a molecular system in which certain holonomic constraints are applied. The leapfrog version of the SHAKE algorithm for propagating a trajectory in an *NVE* ensemble through a time interval Δt reads

$$\tilde{\mathbf{p}}\left(\frac{\Delta t}{2}\right) \leftarrow \mathbf{p}\left(-\frac{\Delta t}{2}\right) - \frac{\partial U}{\partial \mathbf{x}(0)}\Delta t \tag{26}$$

$$\tilde{\mathbf{x}}(\Delta t) \leftarrow \mathbf{x}(0) + \mathbf{M}^{-1}\tilde{\mathbf{p}}\left(\frac{\Delta t}{2}\right)\Delta t \tag{27}$$

DOI: 10.1021/acs.jpca.9b02771
J. Phys. Chem. A 2019, 123, 6056−6079

$$\mathrm{C}_1:\ \begin{cases} \text{solve } \boldsymbol{\lambda}\text{: } \boldsymbol{\sigma}\left(\tilde{\mathbf{x}}(\Delta t) + \mathbf{M}^{-1}\dfrac{\partial \boldsymbol{\sigma}}{\partial \mathbf{x}(0)}\boldsymbol{\lambda}\right) = 0 \\ \mathbf{x}(\Delta t) \leftarrow \tilde{\mathbf{x}}(\Delta t) + \mathbf{M}^{-1}\dfrac{\partial \boldsymbol{\sigma}}{\partial \mathbf{x}(0)}\boldsymbol{\lambda} \\ \mathbf{p}\left(\dfrac{\Delta t}{2}\right) \leftarrow \tilde{\mathbf{p}}\left(\dfrac{\Delta t}{2}\right) + \dfrac{1}{\Delta t}\dfrac{\partial \boldsymbol{\sigma}}{\partial \mathbf{x}(0)}\boldsymbol{\lambda} \end{cases} \tag{28}$$

In "C_1" (eq 28), $\boldsymbol{\lambda}$ is the n_c-dimensional vector of Lagrange multipliers, and the momentum update step (*i.e.*, the last equation of eq 28) can also be replaced by $\mathbf{p}\left(\frac{\Delta t}{2}\right) \leftarrow \tilde{\mathbf{p}}\left(\frac{\Delta t}{2}\right) + \frac{1}{\Delta t}\mathbf{M}(\mathbf{x}(\Delta t) - \tilde{\mathbf{x}}(\Delta t))$ or $\mathbf{p}\left(\frac{\Delta t}{2}\right) \leftarrow \frac{1}{\Delta t}\mathbf{M}(\mathbf{x}(\Delta t) - \mathbf{x}(0))$ (they perform similarly when double-precision numbers are used, but the former is better in a typical single-precision floating-point simulation[50]). The first equation of eq 28 is generally nonlinear. When the system only has triatomic molecules such as water, the equation can be analytically solved by the SETTLE algorithm.[38] For general molecular systems, the first equation of eq 28 can be numerically solved in an iterative fashion using, *e.g.*, Newton's method. In Newton's method, each iteration step (for updating the solution vector $\boldsymbol{\lambda}$) reads

$$\begin{aligned} &\text{solve } \bar{\boldsymbol{\lambda}}\text{: } \left(\frac{\partial \boldsymbol{\sigma}}{\partial \bar{\mathbf{x}}}\right)^T \mathbf{M}^{-1}\frac{\partial \boldsymbol{\sigma}}{\partial \mathbf{x}(0)}\bar{\boldsymbol{\lambda}} = -\boldsymbol{\sigma}(\bar{\mathbf{x}}) \\ &\bar{\mathbf{x}} \leftarrow \bar{\mathbf{x}} + \mathbf{M}^{-1}\frac{\partial \boldsymbol{\sigma}}{\partial \mathbf{x}(0)}\bar{\boldsymbol{\lambda}} \\ &\boldsymbol{\lambda} \leftarrow \boldsymbol{\lambda} + \bar{\boldsymbol{\lambda}} \end{aligned} \tag{29}$$

where the initial values for $\bar{\mathbf{x}}$ and $\boldsymbol{\lambda}$ can be set as $\bar{\mathbf{x}} = \tilde{\mathbf{x}}(\Delta t)$ and $\boldsymbol{\lambda} = 0$, respectively. When the total number of holonomic constraints is relatively small, the full set of the vector $\bar{\boldsymbol{\lambda}}$ (for all constraints) can be simultaneously updated by the LU decomposition. The numerical procedure is known as matrix-SHAKE.[39] When the system involves a large number of constraints and the dimensionality of the matrix equation in eq 29 becomes high, one then often employs a simpler but computationally less intensive iterative approach. For instance, replacing the full matrix $\left(\frac{\partial \boldsymbol{\sigma}}{\partial \bar{\mathbf{x}}}\right)^T \mathbf{M}^{-1}\frac{\partial \boldsymbol{\sigma}}{\partial \mathbf{x}(0)}$ by its diagonal elements in eq 29, one obtains

$$\left.\begin{aligned} &\text{solve } \bar{\lambda}_k\text{: } \left[\sum_{i=1}^{n_k}\left(\frac{\partial \sigma_k}{\partial \bar{x}_i}\right)\frac{1}{m_i}\frac{\partial \sigma_k}{\partial x_i(0)}\right]\bar{\lambda}_k = -\sigma_k(\bar{\mathbf{x}}) \\ &\bar{x}_i \leftarrow \bar{x}_i + \frac{1}{m_i}\frac{\partial \sigma_k}{\partial x_i(0)}\bar{\lambda}_k \ (i = \overline{1, n_k}) \\ &\lambda_k \leftarrow \lambda_k + \bar{\lambda}_k \end{aligned}\right\}(k = \overline{1, n_c}) \tag{30}$$

Here $\bar{x}_i(i = \overline{1, n_k})$ represents the positions of the n_k atoms involved in the kth constraint. One then treats all holonomic constraints in succession (in eq 30) during one cycle of the iteration.[36] The procedure in eq 29 or eq 30 is repeated until some convergence criterion is satisfied for all constraints. The SHAKE algorithm (eqs 26–28) is denoted "C_1-x-p", with the operations in a right-to-left sequence.

The velocity–Verlet version of the RATTLE algorithm for evolving a trajectory of an *NVE* ensemble through a time interval Δt is

$$\tilde{\mathbf{p}}\left(\frac{\Delta t}{2}\right) \leftarrow \mathbf{p}(0) - \frac{\partial U}{\partial \mathbf{x}(0)}\frac{\Delta t}{2} \tag{31}$$

$$\tilde{\mathbf{x}}(\Delta t) \leftarrow \mathbf{x}(0) + \mathbf{M}^{-1}\tilde{\mathbf{p}}\left(\frac{\Delta t}{2}\right)\Delta t \tag{32}$$

$$\mathrm{C}_1:\ \begin{cases} \text{solve } \boldsymbol{\lambda}\text{: } \boldsymbol{\sigma}\left(\tilde{\mathbf{x}}(\Delta t) + \mathbf{M}^{-1}\dfrac{\partial \boldsymbol{\sigma}}{\partial \mathbf{x}(0)}\boldsymbol{\lambda}\right) = 0 \\ \mathbf{x}(\Delta t) \leftarrow \tilde{\mathbf{x}}(\Delta t) + \mathbf{M}^{-1}\dfrac{\partial \boldsymbol{\sigma}}{\partial \mathbf{x}(0)}\boldsymbol{\lambda} \\ \mathbf{p}\left(\dfrac{\Delta t}{2}\right) \leftarrow \tilde{\mathbf{p}}\left(\dfrac{\Delta t}{2}\right) + \dfrac{1}{\Delta t}\dfrac{\partial \boldsymbol{\sigma}}{\partial \mathbf{x}(0)}\boldsymbol{\lambda} \end{cases} \tag{33}$$

$$\tilde{\mathbf{p}}(\Delta t) \leftarrow \mathbf{p}\left(\frac{\Delta t}{2}\right) - \frac{\partial U}{\partial \mathbf{x}(\Delta t)}\frac{\Delta t}{2} \tag{34}$$

$$\mathrm{C}_2:\ \begin{cases} \text{solve } \boldsymbol{\mu}\text{: } \left(\dfrac{\partial \boldsymbol{\sigma}}{\partial \mathbf{x}(\Delta t)}\right)^T \mathbf{M}^{-1}\left(\tilde{\mathbf{p}}(\Delta t) + \dfrac{\partial \boldsymbol{\sigma}}{\partial \mathbf{x}(\Delta t)}\boldsymbol{\mu}\right) = 0 \\ \mathbf{p}(\Delta t) \leftarrow \tilde{\mathbf{p}}(\Delta t) + \dfrac{\partial \boldsymbol{\sigma}}{\partial \mathbf{x}(\Delta t)}\boldsymbol{\mu} \end{cases} \tag{35}$$

In "C_2" (eq 35), $\boldsymbol{\mu}$ is an n_c-dimensional variable. The first equation of eq 35 is equivalent to the linear system of equations

$$\text{solve } \boldsymbol{\mu}\text{: } \left(\frac{\partial \boldsymbol{\sigma}}{\partial \mathbf{x}(\Delta t)}\right)^T \mathbf{M}^{-1}\frac{\partial \boldsymbol{\sigma}}{\partial \mathbf{x}(\Delta t)}\boldsymbol{\mu} = -\left(\frac{\partial \boldsymbol{\sigma}}{\partial \mathbf{x}(\Delta t)}\right)^T \mathbf{M}^{-1}\tilde{\mathbf{p}}(\Delta t) \tag{36}$$

It can be analytically solved for triatomic molecules (e.g., $\mathrm{H_2O}$) by the SETTLE algorithm.[38] When the total number of holonomic constraints in the system is not large, because $\left(\frac{\partial \boldsymbol{\sigma}}{\partial \mathbf{x}(\Delta t)}\right)^T \mathbf{M}^{-1}\frac{\partial \boldsymbol{\sigma}}{\partial \mathbf{x}(\Delta t)}$ is a symmetric and positive-definite matrix, eq 36 can be straightforwardly solved using a Cholesky decomposition. When a significant number of holonomic constraints are imposed on the system, the iterative procedure in eq 35 is not applied to all constraints simultaneously but to each holonomic constraint in succession.[37] That is, in each cycle of the iteration, the momentum and solution vectors are updated by

$$\left.\begin{aligned} &\text{solve } \bar{\mu}_k\text{: } \left[\sum_{i=1}^{n_k}\left(\frac{\partial \sigma_k}{\partial x_i(\Delta t)}\right)^T\frac{1}{m_i}\frac{\partial \sigma_k}{\partial x_i(\Delta t)}\right]\bar{\mu}_k = -\sum_{i=1}^{n_k}\left(\frac{\partial \sigma_k}{\partial x_i(\Delta t)}\right)^T\frac{1}{m_i}\bar{p}_i \\ &\bar{p}_i \leftarrow \bar{p}_i + \left(\frac{\partial \sigma_k}{\partial \mathbf{x}_i(\Delta t)}\right)\bar{\mu}_k (i = \overline{1, n_k}) \\ &\mu_k \leftarrow \mu_k + \bar{\mu}_k \end{aligned}\right\}(k = \overline{1, n_c}) \tag{37}$$

DOI: 10.1021/acs.jpca.9b02771
J. Phys. Chem. A 2019, 123, 6056–6079

Equation 37 is analogous to eq 30 used in the position-constraining step C_1. The process in eq 35 or eq 37 is repeated until all holonomic constraints have converged to within the desired accuracy. The RATTLE algorithm (eqs 31−35) is denoted "C_2-p-C_1-x-p", with the operations in a right-to-left sequence.

It is not difficult to show that the SHAKE and RATTLE algorithms are closely related. As discussed in ref 51, the similarity can be seen from eq 34 and eq 35 of the previous time step that

$$\mathbf{p}(0) \leftarrow \mathbf{p}\left(-\frac{\Delta t}{2}\right) - \frac{\partial U}{\partial \mathbf{x}(0)}\frac{\Delta t}{2} + \frac{\partial \boldsymbol{\sigma}}{\partial \mathbf{x}(0)}\boldsymbol{\mu}_R \tag{38}$$

Substituting eq 38 into eq 31 and then eq 33, one obtains

$$\mathbf{p}\left(\frac{\Delta t}{2}\right) \leftarrow \mathbf{p}\left(-\frac{\Delta t}{2}\right) - \frac{\partial U}{\partial \mathbf{x}(0)}\Delta t + \frac{\partial \boldsymbol{\sigma}}{\partial \mathbf{x}(0)}\left(\frac{\boldsymbol{\lambda}_R}{\Delta t} + \boldsymbol{\mu}_R\right) \tag{39}$$

Comparing eq 39 with the relation from eq 26 and eq 28 in the SHAKE algorithm

$$\mathbf{p}\left(\frac{\Delta t}{2}\right) \leftarrow \mathbf{p}\left(-\frac{\Delta t}{2}\right) - \frac{\partial U}{\partial \mathbf{x}(0)}\Delta t + \frac{\partial \boldsymbol{\sigma}}{\partial \mathbf{x}(0)}\left(\frac{\boldsymbol{\lambda}_S}{\Delta t}\right) \tag{40}$$

One finds that the SHAKE algorithm is equivalent to the RATTLE algorithm at the half step with $\boldsymbol{\lambda}_S = \boldsymbol{\lambda}_R + \boldsymbol{\mu}_R\Delta t$, which is simply a change of variables for the unknown Lagrange multipliers. However, RATTLE satisfies both position and velocity constraints while SHAKE only ensures that the position constraints are satisfied.

2.3. Molecular Dynamics for the *NVT* Ensemble with Holonomic Constraints. *2.3.1. Schemes for Conventional Algorithms.* In the unified thermostat framework,[10,11] many conventional algorithms[52,53] for the *NVT* ensemble with holonomic constraints can be included in the velocity−Verlet version of the "side" scheme (eq 11) by applying the RATTLE algorithm (eqs 31−35). Such a RATTLE version of the "side" scheme reads

thermostat for half a time step $\frac{\Delta t}{2}$ (in which $\mathbf{p}(0)$ is updated) (41)

$$\tilde{\mathbf{p}}\left(\frac{\Delta t}{2}\right) \leftarrow \mathbf{p}(0) - \frac{\partial U}{\partial \mathbf{x}(0)}\frac{\Delta t}{2} \tag{42}$$

$$\tilde{\mathbf{x}}(\Delta t) \leftarrow \mathbf{x}(0) + \mathbf{M}^{-1}\tilde{\mathbf{p}}\left(\frac{\Delta t}{2}\right)\Delta t$$

$$C_1:\begin{cases} \text{solve } \boldsymbol{\lambda}\text{: } \boldsymbol{\sigma}\left(\tilde{\mathbf{x}}(\Delta t) + \mathbf{M}^{-1}\dfrac{\partial \boldsymbol{\sigma}}{\partial \mathbf{x}(0)}\boldsymbol{\lambda}\right) = 0 \\ \mathbf{x}(\Delta t) \leftarrow \tilde{\mathbf{x}}(\Delta t) + \mathbf{M}^{-1}\dfrac{\partial \boldsymbol{\sigma}}{\partial \mathbf{x}(0)}\boldsymbol{\lambda} \\ \mathbf{p}\left(\dfrac{\Delta t}{2}\right) \leftarrow \tilde{\mathbf{p}}\left(\dfrac{\Delta t}{2}\right) + \dfrac{1}{\Delta t}\dfrac{\partial \boldsymbol{\sigma}}{\partial \mathbf{x}(0)}\boldsymbol{\lambda} \end{cases} \tag{43}$$

$$\tilde{\mathbf{p}}(\Delta t) \leftarrow \mathbf{p}\left(\frac{\Delta t}{2}\right) - \frac{\partial U}{\partial \mathbf{x}(\Delta t)}\frac{\Delta t}{2} \tag{44}$$

thermostat for half a time step $\frac{\Delta t}{2}$ (in which $\tilde{\mathbf{p}}(\Delta t)$ is updated) (45)

$$C_2:\begin{cases} \text{solve } \boldsymbol{\mu}\text{: } \left(\dfrac{\partial \boldsymbol{\sigma}}{\partial \mathbf{x}(\Delta t)}\right)^T \mathbf{M}^{-1}\left(\tilde{\mathbf{p}}(\Delta t) + \dfrac{\partial \boldsymbol{\sigma}}{\partial \mathbf{x}(\Delta t)}\boldsymbol{\mu}\right) = 0 \\ \mathbf{p}(\Delta t) \leftarrow \tilde{\mathbf{p}}(\Delta t) + \dfrac{\partial \boldsymbol{\sigma}}{\partial \mathbf{x}(\Delta t)}\boldsymbol{\mu} \end{cases} \tag{46}$$

In the unified framework, we can also include other conventional algorithms[19,54] in the leapfrog version of the "side" scheme (eq 12) by implementing the SHAKE algorithm (eqs 26−28). Such a SHAKE version of the "side" scheme reads

$$\tilde{\mathbf{p}}(0) \leftarrow \mathbf{p}\left(-\frac{\Delta t}{2}\right) - \frac{\partial U}{\partial \mathbf{x}(0)}\frac{\Delta t}{2} \tag{47}$$

thermostat for a full time step Δt (in which $\tilde{\mathbf{p}}(0)$ is updated) (48)

$$\tilde{\mathbf{p}}\left(\frac{\Delta t}{2}\right) \leftarrow \tilde{\mathbf{p}}(0) - \frac{\partial U}{\partial \mathbf{x}(0)}\frac{\Delta t}{2} \tag{49}$$

$$\tilde{\mathbf{x}}(\Delta t) \leftarrow \mathbf{x}(0) + \mathbf{M}^{-1}\tilde{\mathbf{p}}\left(\frac{\Delta t}{2}\right)\Delta t \tag{50}$$

$$C_1:\begin{cases} \text{solve } \boldsymbol{\lambda}\text{: } \boldsymbol{\sigma}\left(\tilde{\mathbf{x}}(\Delta t) + \mathbf{M}^{-1}\dfrac{\partial \boldsymbol{\sigma}}{\partial \mathbf{x}(0)}\boldsymbol{\lambda}\right) = 0 \\ \mathbf{x}(\Delta t) \leftarrow \tilde{\mathbf{x}}(\Delta t) + \mathbf{M}^{-1}\dfrac{\partial \boldsymbol{\sigma}}{\partial \mathbf{x}(0)}\boldsymbol{\lambda} \\ \mathbf{p}\left(\dfrac{\Delta t}{2}\right) \leftarrow \tilde{\mathbf{p}}\left(\dfrac{\Delta t}{2}\right) + \dfrac{1}{\Delta t}\dfrac{\partial \boldsymbol{\sigma}}{\partial \mathbf{x}(0)}\boldsymbol{\lambda} \end{cases} \tag{51}$$

We denote the RATTLE version of the "side" scheme (eqs 41−46) "C_2-T-p-C_1-x-p-T" and the SHAKE version of the "side" scheme (eqs 47−51) "C_1-x-p-T-p", with the operations in a right-to-left sequence. Similarly, the constraint algorithm in ref 52 would be denoted "T-C_2-p-C_1-x-p-T" in the "side" scheme.

2.3.2. Holonomic Constraints in the "Middle" Scheme. Replacing eq 32 by

$$\tilde{\mathbf{x}}\left(\frac{\Delta t}{2}\right) \leftarrow \mathbf{x}(0) + \mathbf{M}^{-1}\tilde{\mathbf{p}}\left(\frac{\Delta t}{2}\right)\frac{\Delta t}{2} \tag{52}$$

thermostat for a full time step Δt $\left(\text{in which } \tilde{\mathbf{p}}\left(\frac{\Delta t}{2}\right) \text{ is updated}\right)$ (53)

$$\tilde{\mathbf{x}}(\Delta t) \leftarrow \tilde{\mathbf{x}}\left(\frac{\Delta t}{2}\right) + \mathbf{M}^{-1}\tilde{\mathbf{p}}\left(\frac{\Delta t}{2}\right)\frac{\Delta t}{2} \tag{54}$$

in eqs 31−35 leads to the counterpart (of RATTLE) in the "middle" scheme for the *NVT* ensemble. We denote it "C_2-p-C_1-x-T-x-p", with the operations in a right-to-left sequence. Similarly, one can replace eq 27 by eqs 52−54 in the SHAKE algorithm (eqs 26−28) to obtain its counterpart in the "middle"

DOI: 10.1021/acs.jpca.9b02771
J. Phys. Chem. A 2019, 123, 6056−6079

Table 1. Tested Algorithms for the "Middle" Schemes for Liquid Water with Constraints

no.	VV-Middle	no.	LF-Middle
1	C_2-p-C_1-x-T-x-p	1	C_2-C_1-x-T-x-p
2	C_2-p-C_2-C_1-x-T-x-p	2	C_2-C_1-x-C_2-T-x-p
3	C_2-p-C_1-x-C_2-T-x-p	3	C_2-C_1-x-T-C_2-x-p
4	C_2-p-C_2-C_1-x-C_2-T-x-p	4	C_2-C_1-x-C_2-T-C_2-x-p
5	C_2-p-C_1-x-T-C_2-x-p	5	C_2-C_1-x-T-x-C_2-p
6	C_2-p-C_2-C_1-x-T-C_2-x-p	6	C_2-C_1-x-C_2-T-x-C_2-p
7	C_2-p-C_1-x-C_2-T-C_2-x-p	7	C_2-C_1-x-T-C_1-x-p
8	C_2-p-C_2-C_1-x-C_2-T-C_2-x-p	8	C_2-C_1-x-C_2-T-C_1-x-p
9	C_2-p-C_1-x-T-x-C_2-p	9	C_2-C_1-x-T-C_2-C_1-x-p
10	C_2-p-C_2-C_1-x-T-x-C_2-p	10	C_2-C_1-x-C_2-T-C_2-C_1-x-p
11	C_2-p-C_1-x-C_2-T-x-C_2-p	11	C_2-C_1-x-T-C_1-x-C_2-p
12	C_2-p-C_2-C_1-x-C_2-T-x-C_2-p	12	C_2-C_1-x-C_2-T-C_1-x-C_2-p
13	C_2-p-C_1-x-T-C_1-x-p	13	C_2-C_1-x-T-C_2-C_1-x-C_2-p
14	C_2-p-C_2-C_1-x-T-C_1-x-p	14	C_2-C_1-x-C_2-T-C_2-C_1-x-C_2-p
15	C_2-p-C_1-x-C_2-T-C_1-x-p		
16	C_2-p-C_2-C_1-x-C_2-T-C_1-x-p		
17	C_2-p-C_1-x-T-C_2-C_1-x-p		
18	C_2-p-C_2-C_1-x-T-C_2-C_1-x-p		
19	C_2-p-C_1-x-C_2-T-C_2-C_1-x-p		
20	C_2-p-C_2-C_1-x-C_2-T-C_2-C_1-x-p		
21	C_2-p-C_1-x-T-C_1-x-C_2-p		
22	C_2-p-C_2-C_1-x-T-C_1-x-C_2-p		
23	C_2-p-C_1-x-C_2-T-C_1-x-C_2-p		
24	C_2-p-C_2-C_1-x-C_2-T-C_1-x-C_2-p		
25	C_2-p-C_1-x-T-C_2-C_1-x-C_2-p		
26	C_2-p-C_2-C_1-x-T-C_2-C_1-x-C_2-p		
27	C_2-p-C_1-x-C_2-T-C_2-C_1-x-C_2-p		
28	C_2-p-C_2-C_1-x-C_2-T-C_2-C_1-x-C_2-p		

scheme for the *NVT* ensemble, which is denoted "C_1-x-T-x-p", with the operations in a right-to-left sequence.

In addition to this straightforward approach to implementing the SHAKE or RATTLE algorithms in the "middle" scheme, we can construct various other versions, in which the position and momentum satisfy the two equations (eqs 24 and 25) for holonomic constraints at the end of the propagation through a time interval Δt. Apparently, the position-constraining step C_1 (eq 28 or eq 33) can be performed after a position-update step "x". Because the momentum-constraining step C_2 (eq 35) does not change the position, it can be implemented after a position-update step "x", a momentum-update step "p", or a thermostat step "T". All possible versions are listed in Table 1, and their applications to the TIP3P model for liquid water and to the Partridge−Schwenke model for a gas phase water molecule are compared in Figures 1−4, as will be discussed in section 3. The results in Figures 1−4 indicate that "C_2-p-C_1-x-T-x-C_2-p" based on the velocity−Verlet version, or "C_2-C_1-x-T-x-C_2-p" derived from the leapfrog version in the "middle" scheme is a reasonably good choice. This simple version only involves one position-constraining step and two momentum-constraining steps in the full propagation for Δt. Specifically, the criterion is that step C_1 (eq 28 or eq 33) is added after "x-T-x" while step C_2 (eq 35) is added after each momentum-update step "p" and at the end of the full integrator for a time interval Δt.

We note that the geodesic BAOAB (g-BAOAB) algorithm proposed in refs 25 and 26 is exactly the same as no. 28 ("C_2-p-C_2-C_1-x-C_2-T-C_2-C_1-x-C_2-p") of the algorithms built upon VV-Middle in the first column of Table 1 when "global" Langevin dynamics is used as the thermostat. That is, the g-BAOAB algorithm[25,26] is a special case of and can be included in no. 28 ("C_2-p-C_2-C_1-x-C_2-T-C_2-C_1-x-C_2-p") of VV-Middle.

Here, an important point about the "middle" scheme with holonomic constraints should be made. Even when no holonomic constraints are applied, for the "VV-Middle" scheme, although its marginal distribution of positions is more accurate, that of momenta is less precise than what the "VV-Side" scheme[8,10] or "VV-End" scheme[10] leads to. Note that in the "VV-Side" or "VV-End" scheme, the thermostat (T) can be applied at the end of the step after the RATTLE (C_2) step. Thermostat operators, such as that for Nosé−Hoover chains, simply scale the momenta, which does not affect the RATTLE step, since this step is linear in the momenta. Therefore, the scaled momenta emerging from the "T" step will satisfy the same constraint condition as they did before, provided that all of the momenta involved in the constraint are coupled to the same thermostat. In the "middle" scheme, the momenta are shifted in the "p" step after they are scaled in the "T" step. Finally, they are adjusted by C_2 to satisfy the time-derivative of the constraint. These adjustments are likely to perturb the momentum fluctuations driven by the thermostat and, hence, the Maxwell distribution of momenta generated by the thermostat. In order to solve this problem, the scaling factors from the thermostat that would be applied to the momenta after the "p" and "C_2" steps would need to be known. However, these cannot be known until the result of the "p" and "C_2" steps on the momenta is known. In principle, this would require a self-consistent iteration "T", "p", and "C_2" steps if one wishes to have consistent satisfaction of the constraints and the scaling of the "T" operator at the end of the whole integration step. This problem may cause difficulty when the constraint force is applied in the first momentum-update step. However, as explicitly discussed in section S1 of the Supporting Information, applying the constraint force in the first momentum-update

DOI: 10.1021/acs.jpca.9b02771
J. Phys. Chem. A 2019, 123, 6056−6079

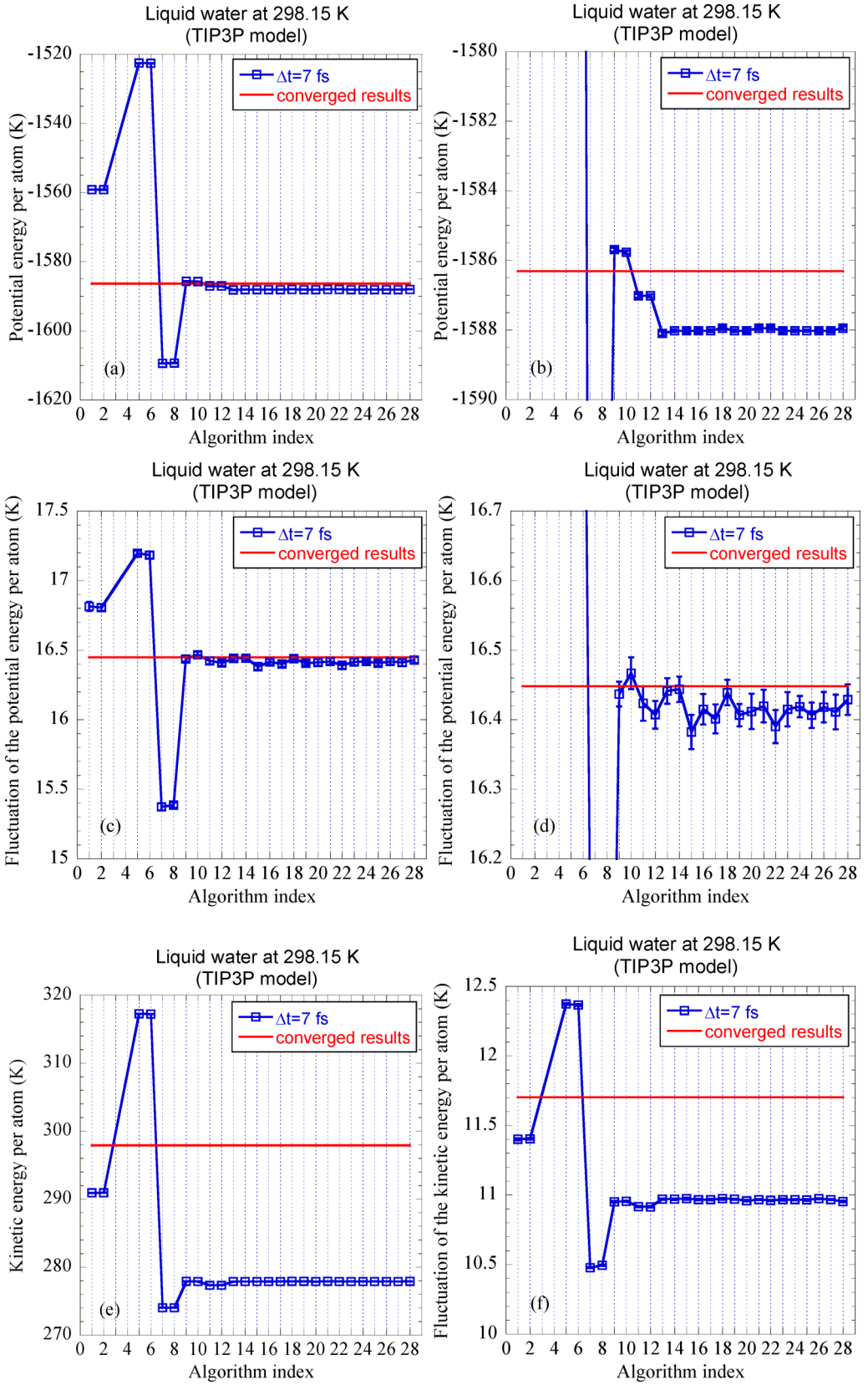

Figure 1. Results with different constraint algorithms of the VV-Middle scheme for liquid water with bond length constraints at 298.15 K. (Blue squares are results obtained with Δt = 7 fs.) All units are kelvin. (a) averaged potential energy per atom $\langle U(\mathbf{x})\rangle/(N_{\text{atom}}k_B)$; (b) enlarged version of panel a; (c) fluctuation of the potential energy per atom $\sqrt{\langle U(\mathbf{x})^2\rangle - \langle U(\mathbf{x})\rangle^2}/(N_{\text{atom}}k_B)$; (d) enlarged version of panel c; (e) averaged kinetic energy per atom $\langle \mathbf{p}^T\mathbf{M}^{-1}\mathbf{p}\rangle/(2N_{\text{atom}}k_B)$; (f) fluctuation of the kinetic energy per atom $\sqrt{\langle(\mathbf{p}^T\mathbf{M}^{-1}\mathbf{p})^2\rangle - \langle \mathbf{p}^T\mathbf{M}^{-1}\mathbf{p}\rangle^2}/(2N_{\text{atom}}k_B)$.

DOI: 10.1021/acs.jpca.9b02771
J. Phys. Chem. A 2019, 123, 6056−6079

step in the "VV-Middle" scheme is *not* the only choice. Choices that are more reasonable are introduced in section S1 of the Supporting Information and used in the paper. On the other hand, if the temperature (estimated from the kinetic energy) is reported immediately after the "T" operator is applied, then the iteration can be avoided at the expense of a small inconsistency between "T" and "C_2" at the end of the step. Another reasonable choice is to use "LF-Middle" rather than "VV-Middle", if the marginal distribution of momenta is concerned. When no holonomic constraints are applied, both "LF-Middle" and "VV-Middle" schemes yield the same (accurate) marginal distribution of positions, but the "LF-Middle" scheme leads to more accurate marginal distribution of momenta than the "VV-Middle" scheme produces.[11] It is easy to prove that "LF-Middle" yields the same marginal distribution of momenta as "PV-End" (position-Verlet end) of ref 34, which has comparable accuracy to that of the conventional "VV-Side" or "VV-End" scheme. (See Figure 2 of ref 34.) Figures 1 and 2 of ref 11 also imply that the accuracy of the marginal distribution of momenta produced by "LF-Middle" is comparable to that yielded by the conventional "side" scheme. For the "LF-Middle" scheme with holonomic constraints, the marginal distribution of momenta in the unconstrained subspace is very close to that of the Maxwell–Boltzmann distribution at the end of the whole integration step, with some possible perturbation due to the last update step for the positions. In some cases (e.g., all momenta are resampled from the Maxwell distribution in each thermostat step "T"), the conventional "end" or "side" scheme with holonomic constraints is probably better for estimating the marginal distribution of momenta than the "LF-Middle" scheme. Generally, since only the positions and not the momenta are needed at the end of the whole step to evaluate equilibrium properties, this technical issue is *not* likely to cause a problem.

2.3.3. Global or Local Thermostats for Holonomic Constraints. Special care should be taken in the thermostat step "T" (i.e., eq 41, eq 45, eq 48 or eq 53) for generating the correct momentum distribution (at the end of the whole integration step for Δt) that is consistent with the holonomic constraint (eq 24) of the system. When a "global" thermostat is employed, i.e., when the momentum for each particle is changed by using the same thermostat parameter(s) in each thermostat step, the numerical integrator for eq 53 for constrained dynamics is similar to that for dynamics with no constraints in cases when the iteration alluded to above is not needed, the only difference being the application of the constraining steps C_1 and C_2. This has already been demonstrated by Lelièvre et al.[55] for Langevin dynamics, as well as by Ryckaert and Ciccotti[56] for the Andersen thermostat and by Kalibaeva et al.[52] for the Nosé–Hoover chain thermostat, for systems with holonomic constraints.

When a "local" thermostat is used for a system with holonomic constraints, however, the numerical integrator for the thermostat step "T" should be modified in order to generate the correct canonical distribution of the momenta. A "local" thermostat implies that the thermostat is applied only to some (randomly) selected degrees of freedom at each thermostat step and that different thermostat parameters are used for different particles (or different degrees of freedom), as in the "massive" Nose–Hoover chain thermostat. One can separate the components of the momentum vector into two subspaces, the constrained subspace $\left\{\mathbf{p}\middle|\left(\frac{\partial\boldsymbol{\sigma}}{\partial\mathbf{x}}\right)^T\mathbf{M}^{-1}\mathbf{p}=0\right\}$ and the unconstrained one. The thermostat process should maintain the Maxwell distribution of the momentum components projected in the unconstrained subspace. This is the most important criterion when a "local" thermostat is employed for the system with holonomic constraints. The simplest way to implement "local" thermostats is to ensure that all momenta in a common constraint are coupled to the same thermostat. However, we propose to lift the restriction and employ the "massive local" thermostat where each degree of freedom is coupled to a different thermostat. The procedure to be discussed in the next paragraph is generally applicable for any type of "local" thermostat, including the "massive" NHC, the resonance-free SIN(R) algorithm, etc.

The constraint for the momentum at position $\mathbf{x}$ can be recast as

$$\left(\frac{\partial\boldsymbol{\sigma}}{\partial\mathbf{x}}\right)^T\mathbf{M}^{-1}\mathbf{p}=\left[\left(\frac{\partial\boldsymbol{\sigma}}{\partial\mathbf{x}}\right)^T\mathbf{M}^{-1/2}\right](\mathbf{M}^{-1/2}\mathbf{p})=0 \tag{55}$$

One can orthogonalize rows of $\left(\frac{\partial\boldsymbol{\sigma}}{\partial\mathbf{x}}\right)^T\mathbf{M}^{-1/2}$ to obtain an orthonormal basis of the momentum space. The orthogonalization procedure can be implemented through a QR decomposition, i.e., by factorizing the matrix $\mathbf{M}^{-1/2}\frac{\partial\boldsymbol{\sigma}}{\partial\mathbf{x}}$ into a product $\mathbf{M}^{-1/2}\frac{\partial\boldsymbol{\sigma}}{\partial\mathbf{x}}=\mathbf{QR}$ of an orthogonal $3N\times 3N$ matrix $\mathbf{Q}$ and a $3N\times n_c$ matrix $\mathbf{R}$ for which $R_{ij}=0$ for all $i>j$. Let $\mathbf{P}=\mathbf{Q}^T\mathbf{M}^{-1/2}\mathbf{p}$. One then obtains

$$\mathbf{R}^T\mathbf{P}=\left(\frac{\partial\boldsymbol{\sigma}}{\partial\mathbf{x}}\right)^T\mathbf{M}^{-1}\mathbf{p} \tag{56}$$

The thermostat process must only be applied to the unconstrained modes of $\mathbf{P}$ ($j=\overline{n_c+1,\,3N}$), leaving the value of $\mathbf{R}^T\mathbf{P}$ unchanged. Although $\mathbf{R}^T\mathbf{P}=0$ is exactly satisfied at the beginning and end of the *full* integrator through a time interval Δt, it is not required that it holds rigorously [i.e., that the constraint for the momentum (eq 57) be exactly satisfied] before the thermostat step "T". The thermostat step for a given time interval δt reads

$$\mathrm{T}:\begin{cases}\mathbf{QR}=\mathbf{M}^{-1/2}\dfrac{\partial\boldsymbol{\sigma}}{\partial\mathbf{x}}\\ \mathbf{P}\leftarrow\mathbf{Q}^T\mathbf{M}^{-1/2}\mathbf{p}\\ P_j\leftarrow Therm(P_j,\,\delta t),\ j=\overline{n_c+1,\,3N}\\ \mathbf{p}\leftarrow\mathbf{M}^{1/2}\mathbf{QP}\end{cases} \tag{57}$$

where the (conventional) thermostat process $Therm(P_j,\,\delta t)$ updates the unconstrained modes P_j ($j=\overline{n_c+1,\,3N}$) while no thermostat process is applied to the constrained modes P_j ($j=\overline{1,\,n_c}$). The Maxwell momentum distribution in the unconstrained subspace then remains invariant after the thermostat process.

$$\exp\left[-\frac{\beta}{2}\sum_{j=n_c+1}^{3N}P_j^2\right]=\exp\left[-\frac{\beta}{2}\mathbf{p}^T\mathbf{M}^{-1/2}\mathbf{Q}\begin{pmatrix}\mathbf{0}_{n_c\times n_c} & \\ & \mathbf{1}_{(3N-n_c)\times(3N-n_c)}\end{pmatrix}\mathbf{Q}^T\mathbf{M}^{-1/2}\mathbf{p}\right] \tag{58}$$

The computational cost for the QR decomposition is $O(3Nn_c^2)$ by using the Householder transformation. An alternative

DOI: 10.1021/acs.jpca.9b02771
J. Phys. Chem. A 2019, 123, 6056–6079

method was previously proposed in ref 57 for "local" stochastic thermostats, which recovers the Maxwell distribution before the thermostat step, and then applies the constraints. The projection method (eq 57) involves the QR factorization and multiplication of matrices and vectors, while the distribution-recovering method introduces additional cost for velocity-constraining steps and the thermostat process for all those degrees of freedom involved in the constraint(s). The projection method (eq 57) is not limited to stochastic thermostats and can also be conveniently used in deterministic thermostats.

Below, we use three typical thermostats as examples for demonstrating algorithms for systems with holonomic constraints.

2.3.3.1. Andersen Thermostat. The thermostat step (with no constraints) in the Andersen thermostat is

$$p_j \leftarrow \sqrt{\frac{m_j}{\beta}}\theta_j, \ \text{if}\ \mu_j < 1 - \mathrm{e}^{-\nu\Delta t}, \ j = \overline{1, 3N} \tag{59}$$

Here ν is the collision frequency, θ_j is an independent Gaussian-distributed random number with zero mean and unit variance, m_j is the mass of the jth degree of freedom, and μ_j is a uniformly distributed random number in the range (0, 1) and may be different for each particle.

The thermostat step in the "local" Andersen thermostat where $\{\mu_j\}$ are not the same for all particles reads

$$\text{T:}\begin{cases} \mathbf{QR} = \mathbf{M}^{-1/2}\dfrac{\partial\boldsymbol{\sigma}}{\partial\mathbf{x}} \\ \mathbf{P} \leftarrow \mathbf{Q}^T\mathbf{M}^{-1/2}\mathbf{p} \\ P_j \leftarrow \sqrt{\dfrac{1}{\beta}}\theta_j, \ \text{if}\ \mu_j < 1 - \mathrm{e}^{-\nu\Delta t}, \ j = \overline{n_c + 1, 3N} \\ \mathbf{p} \leftarrow \mathbf{M}^{1/2}\mathbf{QP} \end{cases} \tag{60}$$

When the Andersen thermostat is applied "globally", $\{\mu_j\}$ is reduced to only one random number μ that determines whether the momentum of all degrees of freedom are changed simultaneously, i.e.,

$$\text{T:}\begin{cases} p_j \leftarrow \sqrt{\dfrac{m_j}{\beta}}\theta_j, \ j = \overline{1, 3N}, \ \text{if}\ \mu < 1 - \mathrm{e}^{-\nu\Delta t} \end{cases} \tag{61}$$

One can straightforwardly implement eq 61, rather than eq 60, in the "global" case for systems with holonomic constraints.

2.3.3.2. Langevin Dynamics. When Langevin dynamics is employed as a thermostat, the thermostat step "T" represents the Ornstein−Uhlenbeck (OU) process, of which the equations of motion are

$$\begin{pmatrix} \dot{\mathbf{x}} \\ \dot{\mathbf{p}} \end{pmatrix} = \begin{pmatrix} \mathbf{0} \\ -\boldsymbol{\gamma}\mathbf{p} + \sqrt{\dfrac{2}{\beta}}\boldsymbol{\gamma}^{1/2}\mathbf{M}^{1/2}\tilde{\boldsymbol{\eta}}(t) \end{pmatrix} \tag{62}$$

where γ is the friction coefficient matrix and $\tilde{\boldsymbol{\eta}}(t)$ is the white-noise term with the correlation function of the elements $\langle\tilde{\eta}_i(t)\tilde{\eta}_j(t')\rangle = \delta_{ij}\delta(t - t')$. The analytical solution to the OU process (eq 62) for a time interval Δt produces

$$\text{T:}\ \mathbf{p} \leftarrow \mathbf{c}_1\mathbf{p} + \mathbf{c}_2\sqrt{\frac{1}{\beta}}\mathbf{M}^{1/2}\boldsymbol{\eta} \tag{63}$$

where the coefficients $\mathbf{c}_1 = e^{-\gamma\Delta t}$ and $\mathbf{c}_2 = (\mathbf{1} - \mathbf{c}_1\mathbf{c}_1^T)^{1/2}$, $\boldsymbol{\eta}$ is the vector of independent Gaussian-distributed random numbers with zero mean and unit variance, which is different for each degree of freedom and each invocation.

When the Langevin thermostat is applied locally for systems with holonomic constraints, the thermostat step becomes

$$\text{T:}\begin{cases} \mathbf{QR} = \mathbf{M}^{-1/2}\dfrac{\partial\boldsymbol{\sigma}}{\partial\mathbf{x}} \\ \mathbf{P} \leftarrow \mathbf{Q}^T\mathbf{M}^{-1/2}\mathbf{p} \\ P_j \leftarrow (\mathbf{Q}^T\mathbf{M}^{-1/2}\mathbf{c}_1\mathbf{M}^{1/2}\mathbf{QP})_j + \sqrt{\dfrac{1}{\beta}}(\mathbf{Q}^T\mathbf{M}^{-1/2}\mathbf{c}_2\mathbf{M}^{1/2}\boldsymbol{\eta})_j, \ j = \overline{n_c + 1, 3N} \\ \mathbf{p} \leftarrow \mathbf{M}^{1/2}\mathbf{QP} \end{cases} \tag{64}$$

where $(\mathbf{Q}^T\mathbf{M}^{-1/2}\mathbf{c}_1\mathbf{M}^{1/2}\mathbf{QP})_j$ or $(\mathbf{Q}^T\mathbf{M}^{-1/2}\mathbf{c}_2\mathbf{M}^{1/2}\boldsymbol{\eta})_j$ represents the jth element of the corresponding vector.

In contrast, when the Langevin thermostat is used globally, i.e., the friction coefficient matrix γ is the product of a scalar parameter and an identity matrix, the thermostat step (the OU process) for systems with holonomic constraints can be the same as the one for systems with no constraints (i.e., eq 63 with γ reduced to a scalar constant).

2.3.3.3. NHC Thermostat. In the "local" NHC thermostat (which is also called the "massive" NHC[7,58]) each degree of freedom is coupled to a different Nosé−Hoover chain. When applied to systems with holonomic constraints, the equations of motion of the "local" NHC are

$$\begin{aligned} \dot{\mathbf{x}} &= \mathbf{M}^{-1}\mathbf{p} \\ \dot{\mathbf{p}} &= -\frac{\partial U(\mathbf{x})}{\partial\mathbf{x}} - \frac{1}{Q_1}\mathbf{M}^{1/2}\mathbf{Q}\,\mathrm{diag}(\mathbf{p}_{\eta_1})\mathbf{Q}^T\mathbf{M}^{-1/2}\mathbf{p} + \frac{\partial\boldsymbol{\sigma}}{\partial\mathbf{x}}\boldsymbol{\lambda} \\ \left.\begin{aligned} \dot{\eta}_j^{(i)} &= \frac{p_{\eta_j^{(i)}}}{Q_j} \\ \dot{p}_{\eta_1^{(i)}} &= P_i^2 - k_\mathrm{B}T - \frac{p_{\eta_2^{(i)}}}{Q_2}p_{\eta_1^{(i)}} \\ \dot{p}_{\eta_j^{(i)}} &= \frac{p^2_{\eta_{j-1}^{(i)}}}{Q_{j-1}} - k_\mathrm{B}T - \frac{p_{\eta_{j+1}^{(i)}}}{Q_{j+1}}p_{\eta_j^{(i)}} (j = \overline{2, M_\mathrm{NHC} - 1}) \\ \dot{p}_{\eta_{M_\mathrm{NHC}}^{(i)}} &= \frac{p^2_{\eta_{M_\mathrm{NHC}-1}^{(i)}}}{Q_{M_\mathrm{NHC}-1}} - k_\mathrm{B}T \end{aligned}\right\} (i = \overline{n_c + 1, 3N}) \end{aligned} \tag{65}$$

DOI: 10.1021/acs.jpca.9b02771
J. Phys. Chem. A 2019, 123, 6056−6079

where diag($\mathbf{p}_{\eta_1}$) ≡ diag{0,···,0, $p_{\eta_1}^{(n_c+1)}$,··· $p_{\eta_1}^{(3N)}$}, and M_{NHC} pairs of additional variables $\{\eta_j^{(i)}, p_{\eta_j}^{(i)}\}(j = \overline{1, M_{\mathrm{NHC}}})$ in the "Nosé−Hoover chain" are coupled only to the unconstrained degree of freedom of the normal-mode momentum $\mathbf{P}_i = (\mathbf{Q}^T\mathbf{M}^{-1/2}\mathbf{p})_i (i = \overline{n_c + 1, 3N})$. For the equations of motion in eq 65, the conserved quantity is

$$H' = \frac{1}{2}\mathbf{p}^T\mathbf{M}^{-1}\mathbf{p} + U(\mathbf{x}) + \sum_{i=n_c+1}^{3N}\sum_{j=1}^{M_{\mathrm{NHC}}}\left(\frac{p_{\eta_j}^{2(i)}}{2Q_j} + k_{\mathrm{B}}T\eta_j^{(i)}\right) \tag{66}$$

When the "local" NHC is used, the algorithm for the thermostat part for a finite time interval Δt reads

$$\left.\begin{aligned}
p_{\eta_{M_{\mathrm{NHC}}}^{(i)}} &\leftarrow p_{\eta_{M_{\mathrm{NHC}}}^{(i)}} + G_{M_{\mathrm{NHC}}}^{(i)}\frac{\delta_\alpha}{2}\\
p_{\eta_j^{(i)}} &\leftarrow p_{\eta_j^{(i)}}\exp\left(-\frac{p_{\eta_{j+1}^{(i)}}}{Q_{j+1}}\frac{\delta_\alpha}{4}\right)\\
p_{\eta_j^{(i)}} &\leftarrow p_{\eta_j^{(i)}} + G_j^{(i)}\frac{\delta_\alpha}{2}\\
p_{\eta_j^{(i)}} &\leftarrow p_{\eta_j^{(i)}}\exp\left(-\frac{p_{\eta_{j+1}^{(i)}}}{Q_{j+1}}\frac{\delta_\alpha}{4}\right)
\end{aligned}\right\}(j = \overline{M_{\mathrm{NHC}} - 1, 1})$$

$$\eta_j^{(i)} \leftarrow \eta_j^{(i)} + \frac{p_{\eta_j^{(i)}}}{Q_j}\delta_\alpha(j = \overline{1, M_{\mathrm{NHC}}})$$

$$P_i \leftarrow P_i\exp\left(-\frac{p_{\eta_1^{(i)}}}{Q_1}\delta_\alpha\right)$$

$$\left.\begin{aligned}
p_{\eta_j^{(i)}} &\leftarrow p_{\eta_j^{(i)}}\exp\left(-\frac{p_{\eta_{j+1}^{(i)}}}{Q_{j+1}}\frac{\delta_\alpha}{4}\right)\\
p_{\eta_j^{(i)}} &\leftarrow p_{\eta_j^{(i)}} + G_j^{(i)}\frac{\delta_\alpha}{2}\\
p_{\eta_j^{(i)}} &\leftarrow p_{\eta_j^{(i)}}\exp\left(-\frac{p_{\eta_{j+1}^{(i)}}}{Q_{j+1}}\frac{\delta_\alpha}{4}\right)
\end{aligned}\right\}(j = \overline{1, M_{\mathrm{NHC}} - 1})$$

$$p_{\eta_{M_{\mathrm{NHC}}}^{(i)}} \leftarrow p_{\eta_{M_{\mathrm{NHC}}}^{(i)}} + G_{M_{\mathrm{NHC}}}^{(i)}\frac{\delta_\alpha}{2}$$

$$\left.\begin{aligned}
&(\alpha = \overline{1, n_{\mathrm{SY}}})\\
&(k = \overline{1, n_{\mathrm{RESPA}}})\\
&(i = \overline{n_c + 1, 3N})
\end{aligned}\right\} \tag{67}$$

where

$$\left.\begin{aligned}
G_1^{(i)} &= P_i^2 - k_{\mathrm{B}}T\\
G_j^{(i)} &= \frac{p_{\eta_{j-1}^{(i)}}^2}{Q_{j-1}} - k_{\mathrm{B}}T(j = \overline{2, M_{\mathrm{NHC}}})
\end{aligned}\right\}(i = \overline{n_c + 1, 3N}) \tag{68}$$

Here, we use RESPA[17,59] to divide an integration step for the NHC thermostat into n_{RESPA} equal parts, and implement the Suzuki−Yoshida decomposition framework[60−62] to further divide each part into n_{SY} smaller parts with different weights $\{w_\alpha\}$. The value of n_{SY} depends on the order of the Suzuki−Yoshida decomposition. Throughout the paper, the sixth order Suzuki−Yoshida factorization is employed. In this case, $n_{\mathrm{SY}} = 7$ and

$$\begin{aligned}
w_1 &= w_7 = 0.784513610477560\\
w_2 &= w_6 = 0.235573213359357\\
w_3 &= w_5 = -1.17767998417887\\
w_4 &= 1 - w_1 - w_2 - w_3 - w_5 - w_6 - w_7
\end{aligned} \tag{69}$$

The parameter

$$\delta_\alpha = \frac{w_\alpha}{n_{\mathrm{RESPA}}}\Delta t \tag{70}$$

is the time step size for the α-th of the n_{SY} smaller parts.

In contrast, in the "global" NHC the whole system is coupled to only one chain.[7] The equations of motion for the "global" NHC are

$$\begin{aligned}
\dot{\mathbf{x}} &= \mathbf{M}^{-1}\mathbf{p}\\
\dot{\mathbf{p}} &= -\frac{\partial U(\mathbf{x})}{\partial \mathbf{x}} - \frac{p_{\eta_1}}{Q_1}\mathbf{p} + \frac{\partial \boldsymbol{\sigma}}{\partial \mathbf{x}}\boldsymbol{\lambda}\\
\dot{\eta}_j &= \frac{p_{\eta_j}}{Q_j}(j = \overline{1, M_{\mathrm{NHC}}})\\
\dot{p}_{\eta_1} &= \sum_{i=1}^{3N}\frac{p_i^2}{m_i} - (3N - n_c)k_{\mathrm{B}}T - \frac{p_{\eta_2}}{Q_2}p_{\eta_1}\\
\dot{p}_{\eta_j} &= \frac{p_{\eta_{j-1}}^2}{Q_{j-1}} - k_{\mathrm{B}}T - \frac{p_{\eta_{j+1}}}{Q_{j+1}}p_{\eta_j}(j = \overline{2, M_{\mathrm{NHC}} - 1})\\
\dot{p}_{\eta_{M_{\mathrm{NHC}}}} &= \frac{p_{\eta_{M_{\mathrm{NHC}}-1}}^2}{Q_{M_{\mathrm{NHC}}-1}} - k_{\mathrm{B}}T
\end{aligned} \tag{71}$$

When the "global" NHC is used for systems with holonomic constraints, the algorithm for the thermostat part in the "global" NHC for a finite time step Δt reads

$$\left.\begin{aligned}
p_{\eta_{M_{\mathrm{NHC}}}} &\leftarrow p_{\eta_{M_{\mathrm{NHC}}}} + G_{M_{\mathrm{NHC}}}\frac{\delta_\alpha}{2}\\
p_{\eta_j} &\leftarrow p_{\eta_j}\exp\left(-\frac{p_{\eta_{j+1}}}{Q_{j+1}}\frac{\delta_\alpha}{4}\right)\\
p_{\eta_j} &\leftarrow p_{\eta_j} + G_j\frac{\delta_\alpha}{2}\\
p_{\eta_j} &\leftarrow p_{\eta_j}\exp\left(-\frac{p_{\eta_{j+1}}}{Q_{j+1}}\frac{\delta_\alpha}{4}\right)
\end{aligned}\right\}(j = \overline{M_{\mathrm{NHC}} - 1, 1})$$

$$\eta_j \leftarrow \eta_j + \frac{p_{\eta_j}}{Q_j}\delta_\alpha(j = \overline{1, M_{\mathrm{NHC}}})$$

$$p_i \leftarrow p_i\exp\left(-\frac{p_{\eta_1}}{Q_1}\delta_\alpha\right)$$

$$\left.\begin{aligned}
p_{\eta_j} &\leftarrow p_{\eta_j}\exp\left(-\frac{p_{\eta_{j+1}}}{Q_{j+1}}\frac{\delta_\alpha}{4}\right)\\
p_{\eta_j} &\leftarrow p_{\eta_j} + G_j\frac{\delta_\alpha}{2}\\
p_{\eta_j} &\leftarrow p_{\eta_j}\exp\left(-\frac{p_{\eta_{j+1}}}{Q_{j+1}}\frac{\delta_\alpha}{4}\right)
\end{aligned}\right\}(j = \overline{M_{\mathrm{NHC}} - 1, 1})$$

$$p_{\eta_{M_{\mathrm{NHC}}}} \leftarrow p_{\eta_{M_{\mathrm{NHC}}}} + G_{M_{\mathrm{NHC}}}\frac{\delta_\alpha}{2}$$

$$\left.\begin{aligned}
&(\alpha = \overline{1, n_{\mathrm{SY}}})\\
&(k = \overline{1, n_{\mathrm{RESPA}}})\\
&(i = \overline{1, 3N})
\end{aligned}\right\} \tag{72}$$

DOI: 10.1021/acs.jpca.9b02771
J. Phys. Chem. A 2019, 123, 6056−6079

where

$$\left.\begin{aligned} G_1 &= \sum_{i=1}^{3N} \frac{p_i^2}{m_i} - (3N - n_c)k_B T \\ G_j &= \frac{p_{\eta_{j-1}}^2}{Q_{j-1}} - k_B T (j = \overline{2, M_{NHC}}) \end{aligned}\right\} (i = \overline{1, 3N}) \quad (73)$$

3. RESULTS AND DISCUSSION FOR MOLECULAR DYNAMICS WITH HOLONOMIC CONSTRAINTS

3.1. Numerical Performance of the Algorithms in the "Middle" Scheme. As described in section 2.3, various ways exist for inserting the position-constraining step C_1 and the momentum-constraining step C_2 into the unstrained MD integrator(s) such that the two equations (eqs 24 and 25) for the holonomic constraint are satisfied at the end of the propagation through a time interval Δt. Table 1 lists all possible versions built upon the SHAKE/RATTLE algorithms in the "middle" scheme. We have implemented all these versions into the molecular simulation software AMBER (version 2018) to investigate the numerical performance. We have run MD simulations for liquid water at T = 298.15 K for a system of 216 water molecules in a box with periodic boundary conditions applied using the minimum image convention. The TIP3P force field is employed for the water model. We use "global" Langevin dynamics in the thermostat step "T", where the friction coefficient is γ = 5 ps^{-1} for all degrees of freedom. The O−H bond lengths are constrained at 0.9572 Å. The H−O−H angles are constrained at 104.49 degrees. After equilibrating the system for 500 ps, 20 MD trajectories with each propagated up to ∼5 ns are used for estimating thermodynamic properties. The time interval is Δt = 7 fs that is close to the largest possible value for the numerically stable evolution of the MD trajectory. The converged results are obtained with the time interval Δt = 0.5 fs, which are used for the reference for comparing the numerical behaviors of all versions in Table 1. Figures 1 and 2 demonstrate that most versions perform similarly, even when the time interval Δt is large. It is interesting to see in Figure 1 that no. 28 ("C_2-p-C_2-C_1-x-C_2-T-C_2-C_1-x-C_2-p") in the first column of Table 1 (which, since "global" Langevin dynamics is used, is equivalent to the g-BAOAB algorithm of refs 25 and 26) does *not* demonstrate better performance than most other versions in configurational sampling.

We have also tested other liquid water models, including the POLI2VS model-a polarizable and flexible force field for liquid water.[63] The results are very similar to those in Figures 1 and 2. (See section S3 of the Supporting Information).

In addition to liquid water, we test all versions in Table 1 for a gas-phase system—a single H_2O molecule at 300 K. We use the accurate potential energy surface developed by Partridge and Schwenke from extensive ab initio calculations and experimental data.[64] As the explicit form of the PES is available, the forces can be computed analytically. The O−H bond lengths are constrained at 0.95784 Å, leaving the bond angle unconstrained. The "global" Langevin thermostat is employed, where the friction coefficient γ is ∼830 ps^{-1} (0.02 au) for all degrees of freedom. After equilibrating the system, 100 trajectories with each propagated up to ∼2.4 ns are used for estimating the energies. In Figure 3 and Figure 4, the results obtained from the algorithms (of Table 1) are compared for $\Delta t \simeq$ 6.41 fs (265 au), which is a time interval close to the largest value for numerically stably propagating a MD trajectory. The converged data are obtained with the time interval at ∼0.24 fs (10 au), which are used as a reference for comparison. Figure 3 implies that no. 28 ("C_2-p-C_2-C_1-x-C_2-T-C_2-C_1-x-C_2-p") in the first column of Table 1 (i.e., g-BAOAB when the global Langevin thermostat is used) does not necessarily perform better in configurational sampling than most other versions based on "VV-Middle". The error of a single gas-phase H_2O molecule in Figures 3 and 4 is much larger compared to that of liquid water in Figures 1 and 2. This is because all intermolecular modes are frozen in the liquid water simulation while the H−O−H angle bending motion is allowed in the simulation of a single gas-phase H_2O molecule. The intramolecular interaction energy (per atom) is significantly larger than the intermolecular interaction energy (per atom).

Figures 1-4 demonstrate that it is not necessary to apply constraints after every substep ("x", "p", or "T") during the propagation through a time interval Δt. We note that the version (in Table 1) that will exhibit the best performance will depend on the specific system of interest, but most versions produce comparable accuracy. Because the constraining steps C_1 and C_2 often involve additional computational overhead, it is preferable to include as few of these as possible so long as acceptable accuracy is obtained. This is our criterion used for selecting the algorithm. For the purpose of configurational sampling, Figure 1 and Figure 3 demonstrate that no. 9 ("C_2-p-C_1-x-T-x-C_2-p") of those versions constructed upon VV-Middle (in the first column of Table 1) is a reasonably good choice, while Figure 2 and Figure 4 suggest that no. 5 ("C_2-C_1-x-T-x-C_2-p") of the versions derived from LF-Middle (in the second column of Table 1) is a useful option. (Note that most *NVT* ensembles of interest are for condensed phase systems.) Throughout the rest of the paper, for MD with holonomic constraints, we use "C_2-p-C_1-x-T-x-C_2-p" (no. 9 of the first column) as the default VV-Middle version and "C_2-C_1-x-T-x-C_2-p" (no. 5 of the second column) as the default LF-Middle version.

3.2. Comparison between Conventional Algorithms and Those in the "Middle" Scheme for Holonomic Constraints. We then apply the "middle" scheme to several typical systems with holonomic constraints, including a model system, liquid water, and a biological molecule (alanine dipeptide) solvated in implicit solvent. For comparison we also apply the RATTLE version of the "side" scheme ("C_2-T-p-C_1-x-p-T" as described by eqs 41−46), as well as the "default" Langevin thermostat algorithm for constrained MD in the AMBER molecular simulation software (i.e., set the flag ntt = 3 in AMBER). The latter employs the BBK algorithm[19,65]

$$\tilde{\mathbf{p}}\left(\frac{\Delta t}{2}\right) = \frac{1 - \gamma^{BBK}\Delta t/2}{1 + \gamma^{BBK}\Delta t/2}\mathbf{p}\left(-\frac{\Delta t}{2}\right) + \frac{\Delta t}{1 + \gamma^{BBK}\Delta t/2}\left(-\frac{\partial U}{\partial \mathbf{x}(0)} + \sqrt{\frac{2\gamma^{BBK}}{\beta \Delta t}}\mathbf{M}^{1/2}\boldsymbol{\eta}\right)$$

$$\tilde{\mathbf{x}}(\Delta t) = \mathbf{x}(0) + \mathbf{M}^{-1}\tilde{\mathbf{p}}\left(\frac{\Delta t}{2}\right)\Delta t$$

$$C_1: \begin{cases} \text{solve } \lambda: \boldsymbol{\sigma}\left(\tilde{\mathbf{x}}(\Delta t) + \mathbf{M}^{-1}\dfrac{\partial \boldsymbol{\sigma}}{\partial \mathbf{x}(0)}\lambda\right) = 0 \\ \mathbf{x}(\Delta t) \leftarrow \tilde{\mathbf{x}}(\Delta t) + \mathbf{M}^{-1}\dfrac{\partial \boldsymbol{\sigma}}{\partial \mathbf{x}(0)}\lambda \\ \mathbf{p}\left(\dfrac{\Delta t}{2}\right) \leftarrow \tilde{\mathbf{p}}\left(\dfrac{\Delta t}{2}\right) + \dfrac{1}{\Delta t}\dfrac{\partial \boldsymbol{\sigma}}{\partial \mathbf{x}(0)}\lambda \end{cases} \quad (74)$$

DOI: 10.1021/acs.jpca.9b02771
J. Phys. Chem. A 2019, 123, 6056−6079

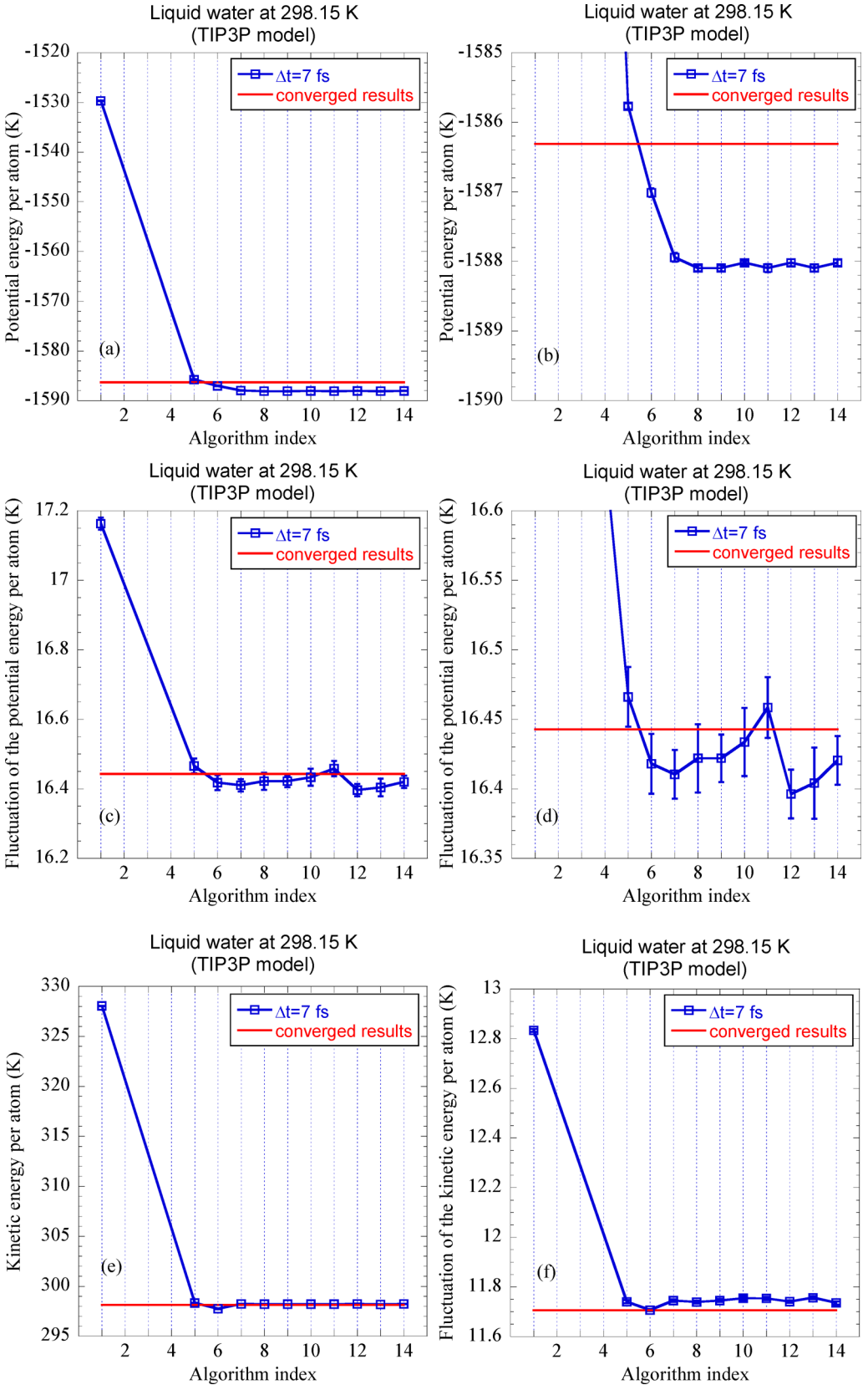

Figure 2. Same as Figure 1, but for the LF-Middle scheme.

where γ^{BBK} is the "global" friction parameter in the BBK algorithm, $\boldsymbol{\eta}$ is the vector of independent Gaussian-distributed random numbers as already defined in eq 63. Given the unified thermostat framework,[10,11,34] it is straightforward to prove that the BBK algorithm (eq 74) is equivalent to the SHAKE version of the "side" scheme ("C_1-x-p-T-p" as described by eqs 47−51), when one uses the "global" Langevin thermostat with the conventional friction constant γ satisfying the relation

DOI: 10.1021/acs.jpca.9b02771
J. Phys. Chem. A 2019, 123, 6056−6079

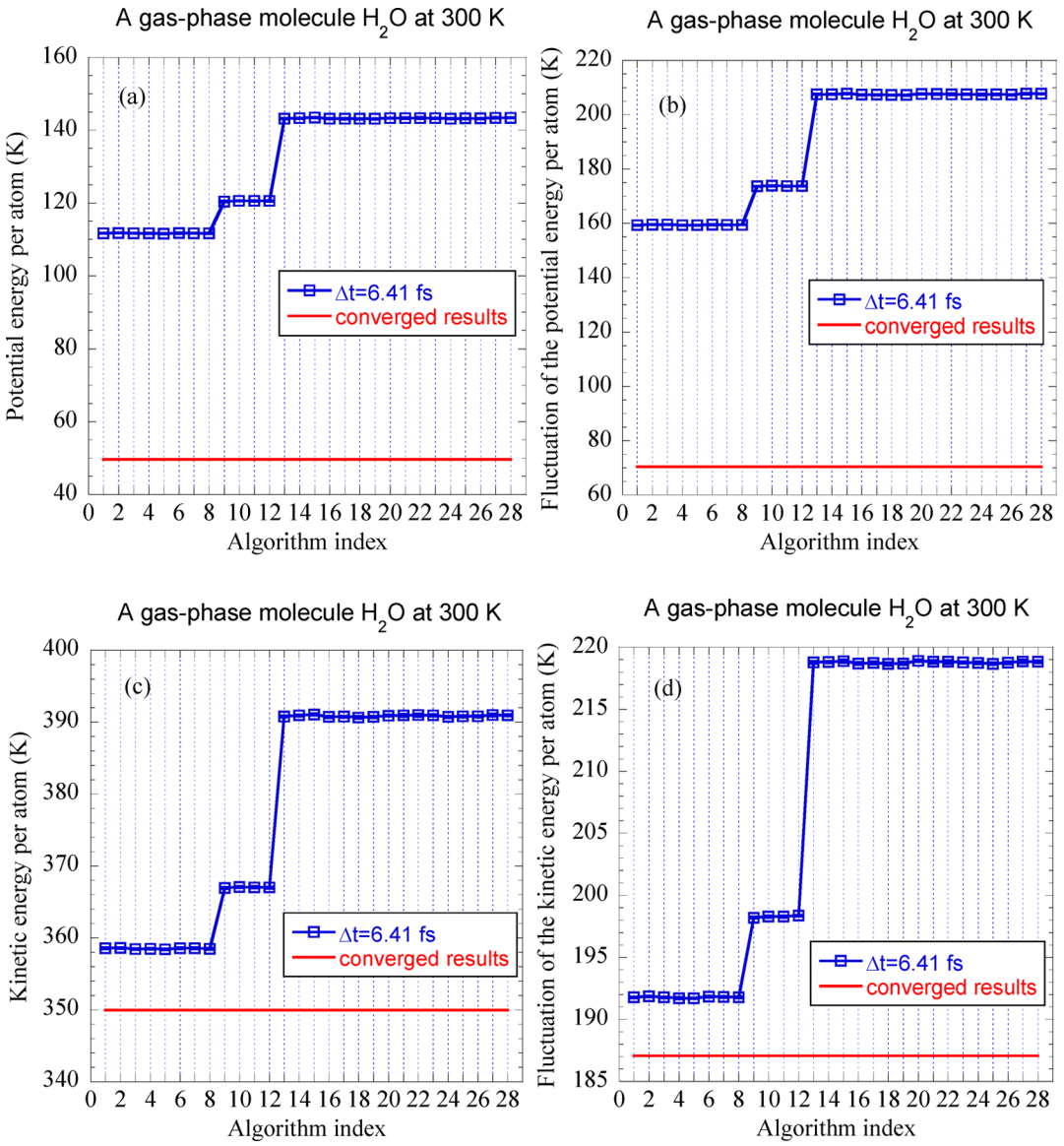

Figure 3. Same as Figure 1, but for a single gas phase H_2O molecule at 300 K, without enlarged panels. (Blue squares are results obtained with Δt = 6.41 fs.)

$$\gamma^{BBK} = \frac{2}{\Delta t}(1 + e^{-\gamma \Delta t})^{-1}(1 - e^{-\gamma \Delta t}) \tag{75}$$

That is, the BBK algorithm is simply a special "global" Langevin dynamics algorithm in the SHAKE version of the "side" scheme of the unified thermostat framework.[10,11,34]

3.2.1. Harmonic System Subject to a Linear Constraint. Consider a harmonic system consisting of two 1-dimensional particles (masses are 1 au, characteristic frequencies ω = 1 au, at inverse temperature β = 1)

$$U(\mathbf{x}) = \frac{1}{2}x_1^2 + \frac{1}{2}x_2^2 \tag{76}$$

The constraint function is

$$\sigma(\mathbf{x}) = x_1 - x_2 \tag{77}$$

For demonstration, we implement the "global" Langevin thermostat with the friction coefficient γ = 1 au, as well as the "local" Andersen thermostat with the collision frequency ν = 1 au and the "massive" NHC thermostat with the inverse of characteristic time $\tau^{-1} = (20\Delta t)^{-1}$ au. Figure 5 shows that the algorithms derived in the "VV-Middle" scheme lead to accurate averaged potential energy results that are relatively insensitive to the time interval, while the "side" scheme does progressively worse as Δt increases, regardless of which type of thermostat is employed. This agrees with the conclusion for cases with no constraints presented in our previous papers.[8,10,11,34,35]

3.2.2. Liquid Water (POLI2VS Model) with Constrained Bond Lengths. We use a flexible and polarizable force field—the POLI2VS model for liquid water.[63] MD simulations are carried out at T = 298.15 K for a system of 216 water molecules in a box with periodic boundary conditions applied using the minimum image convention. The density of liquid water is 0.997 g·cm^{-3}. The charge−charge, charge−dipole and dipole−dipole interactions are treated using the Ewald summation, while the repulsion−dispersion forces and the electrostatic interactions including quadrupoles are cut off from 9.0 to 9.1 Å with the smoothing function. We employ the "global" Langevin thermostat with the friction coefficient γ = 8 ps^{-1}, as well as the

DOI: 10.1021/acs.jpca.9b02771
J. Phys. Chem. A 2019, 123, 6056−6079

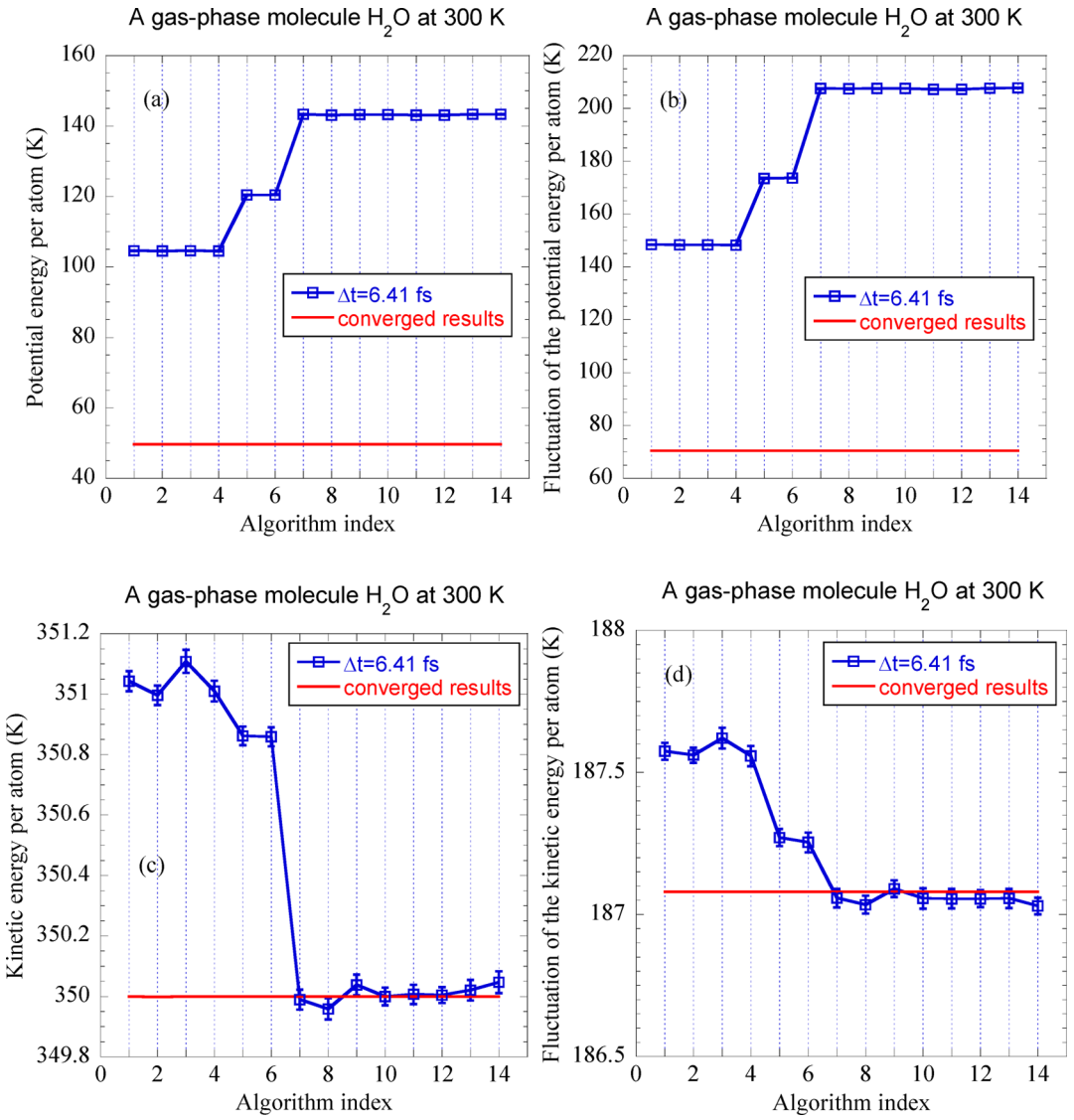

Figure 4. Same as Figure 3, but for the LF-Middle scheme.

"local" Andersen thermostat with the collision frequency ν = 5 ps^{-1} and the "massive" NHC thermostat with the inverse of characteristic time τ^{-1} = 2.84968 ps^{-1}. After equilibrating the system, 20 MD trajectories with each propagated up to 100 ps are used for estimating thermodynamic properties. When O−H bond lengths are constrained, the values of two O−H bond lengths of each water molecule are fixed at 0.917 Å—the optimal O−H bond length for a water monomer. Figure 6 shows that "VV-middle" is more accurate than the "side" scheme for the potential energy results as the time interval increases, irrespective of which type of thermostat is used.

3.2.3. Liquid Water (qSPC/Fw Model) with Constrained Bond Lengths and Constrained Bond Angles. We have implemented both velocity−Verlet and leapfrog versions of the "middle" scheme in AMBER (2018 version). The q-SPC/Fw liquid water model[66] in AMBER is used for testing the performance. The temperature is T = 298.15 K and the density is 0.997 g·cm^{-3}. Classical *NVT* simulations are carried out for a system of 216 water molecules in a box with periodic boundary conditions applied using the minimum image convention. In each molecule, the two O−H bond lengths are constrained at 1.0 Å, and the bond angle H−O−H is constrained at 109.47 deg. We compare the numerical behavior of four thermostat schemes, which are the "default" scheme in AMBER[67] with Langevin thermostat (the BBK algorithm), "LF-Middle", "VV-Middle", and "Side" (i.e., "C_2-T-p-C_1-x-p-T"). The thermostat in each of the last three schemes also employs "global" Langevin dynamics. The thermostat parameter (friction coefficient γ) is 5 ps^{-1} for all the particles in the simulations. After equilibrating the system, 20 MD trajectories with each propagated up to 2 ns are used for estimating thermodynamic properties. Figure 7a indicates that either version in the "middle" scheme is superior to both the "default" Langevin thermostat algorithm[19] in AMBER and the "side" scheme for sampling the marginal distribution of the configuration for the constrained system. Figure 7b also demonstrates that "LF-Middle" leads to a reasonably accurate estimation of the kinetic energy.

3.2.4. Alanine Dipeptide Solvated in Implicit Solvent. We use AMBER (2018 version) to run simulations for alanine dipeptide solvated in implicit solvent of the generalized Born (GB) model.[68−70] Both the default Langevin thermostat algorithm[19] of AMBER and "VV-Middle" are used. The "global" Langevin thermostat is employed with the friction

DOI: 10.1021/acs.jpca.9b02771
J. Phys. Chem. A 2019, 123, 6056−6079

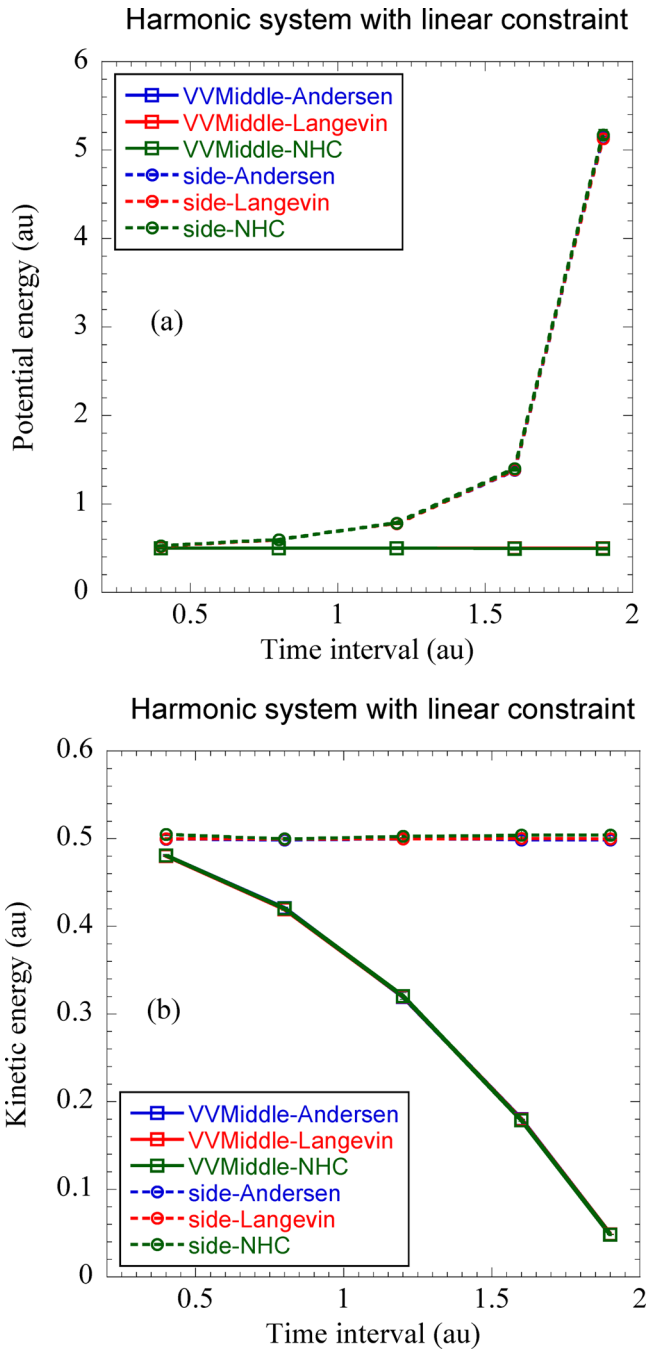

Figure 5. MD results for the two-dimensional harmonic system with linear constraints: (a) averaged potential energy (unit: au) and (b) averaged kinetic energy (unit: au). Statistical error bars are included.

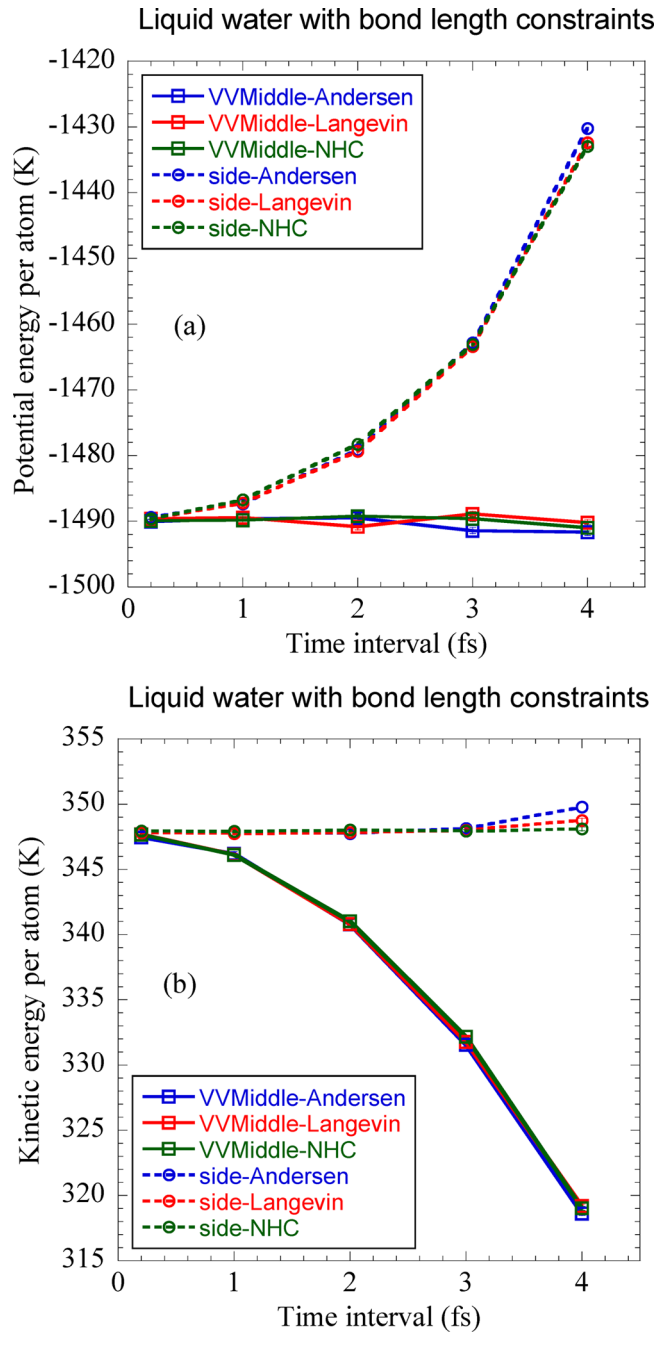

Figure 6. MD results using different schemes for liquid water with O−H bond length constraints using the POLI2VS force field at 298.15 K: (a) averaged potential energy per atom $\langle U(\mathbf{x})\rangle/(N_{\text{atom}}k_B)$ (unit: kelvin) and (b) averaged kinetic energy per atom $\langle \mathbf{p}^T\mathbf{M}^{-1}\mathbf{p}\rangle/(2N_{\text{atom}}k_B)$ (unit: kelvin).

coefficient γ = 1 ps^{-1} for all the particles. Replica exchange molecular dynamics (REMD)[71] is used for accelerating the sampling. We employ 10 temperatures from 273 to 600 K by equally distributing the inverse temperature. The replica exchange is performed every 20 ps. After equilibration of the system for 1 μs, 20 REMD trajectories with each propagated up to 2 μs are used for estimating the properties. Bond length constraints are applied to the bonds that contain hydrogen atoms. The potential of mean force (PMF) for the ψ torsion angle at 300 K (as shown in Figure 8) is calculated using the weighted histogram analysis method (WHAM).[72] As shown in Figure 9 on the PMF barriers and Figure 10 on the average potential energy and its fluctuation, the "middle" scheme leads to accurate results that are relatively insensitive to the time interval, while the "default" scheme in AMBER becomes progressively less accurate as Δt increases. When the time interval Δt is 3 fs, the "middle" scheme still produces accurate results at the same temperature. In contrast, as shown in Figure 10 the deviation of the result produced the "default" scheme in AMBER with Δt = 3 fs from the converged one at the same temperature can be even larger than the difference between the converged result and the one at its neighbor temperature.

DOI: 10.1021/acs.jpca.9b02771
J. Phys. Chem. A 2019, 123, 6056−6079

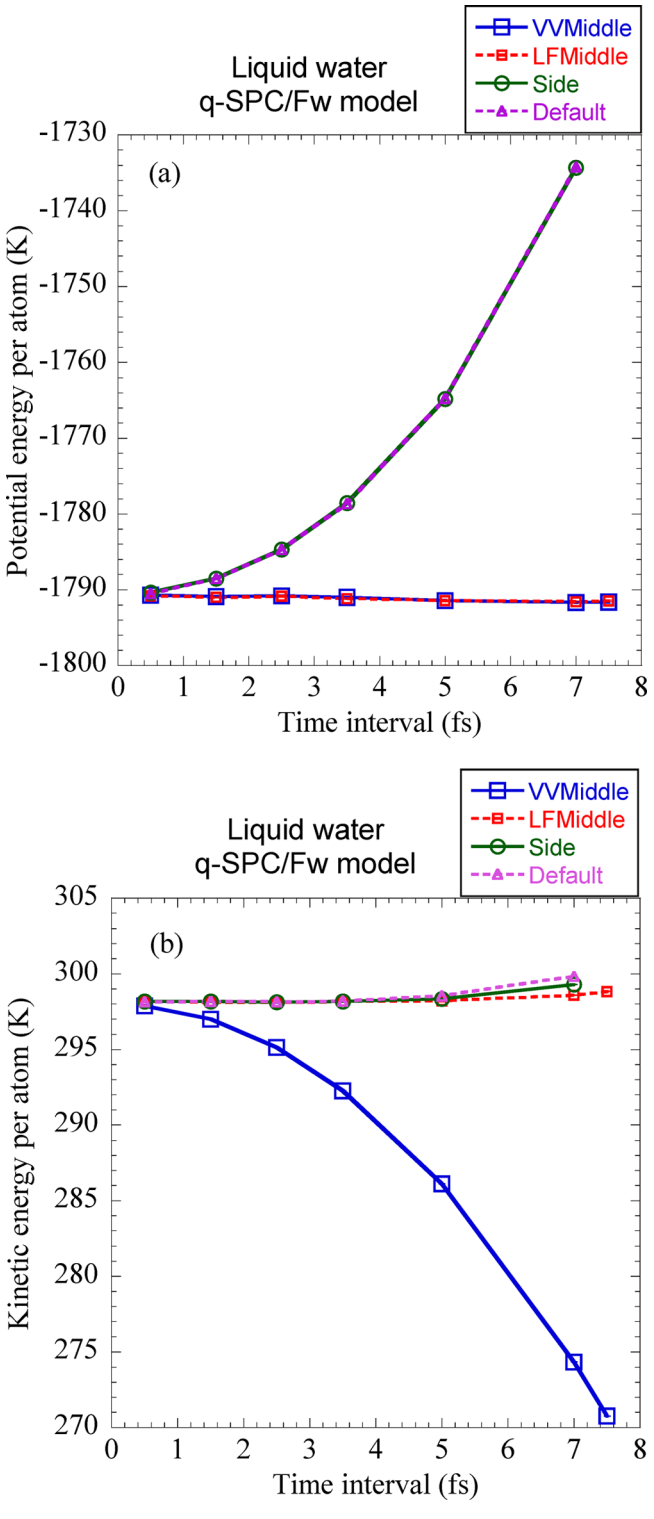

Figure 7. Same as Figure 6, but for liquid water system with bond length constraints for bonds containing hydrogen atom using q-SPC/Fw force field model.

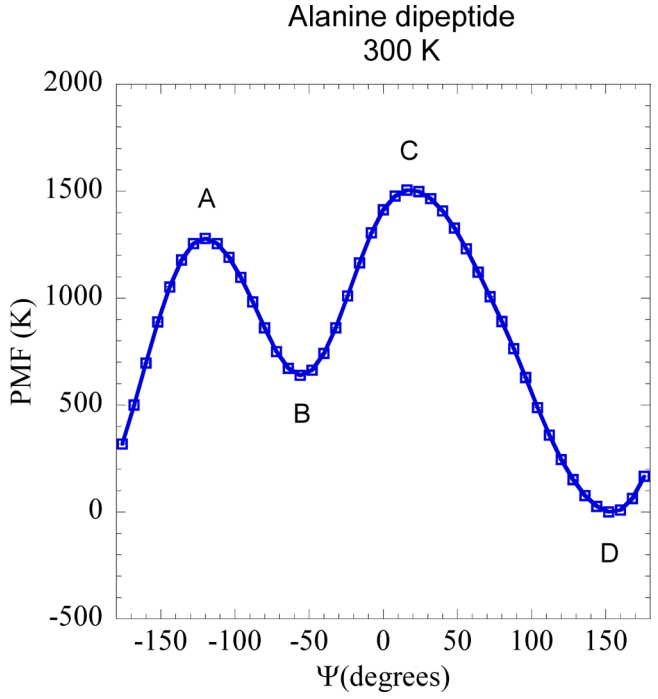

Figure 8. Potential of mean force (PMF) for the torsion angle ψ for alanine dipeptide solvated in an implicit solvent model at 300 K, (Unit: kelvin).

4. THEORY FOR ISOKINETIC CONSTRAINTS IN THE "MIDDLE" SCHEME

Nonholonomic constraints that include momenta as variables are also widely used in MD for the *NVT* ensemble. Here we use the isokinetic constraint as an example to demonstrate the application of the "middle" thermostat scheme. Minary et al. introduced Iso-NHC-RESPA,[47] a MTS (multiple time-step) algorithm originated from the reference system propagator algorithm (RESPA),[17,59] based on the NHC approach combined with a set of isokinetic constraints which controls resonance problem thereby allowing an increase in the outer time step in MTS schemes. Leimkuhler et al. replaced the thermostat chains in the Iso-NHC-RESPA scheme with the Nosé−Hoover−Langevin method,[73] which allows an increase in the efficiency without a reduction in the outer time step. This method is referred as Stochastic-Iso-NH-RESPA [SIN(R)].[49] In the paper we focus on SIN(R).

Consider a system with the Hamiltonian in eq 1. For each degree of freedom $i = \overline{1, 3N}$ of the system, a system of stochastic equations of motion is introduced as

$$\dot{x}_i = \frac{p_i}{m_i}$$

$$\dot{p}_i = -\frac{\partial U}{\partial x_i} - \lambda_i p_i$$

$$\dot{v}_{1,i}^{(k)} = -\lambda_i v_{1,i}^{(k)} - v_{2,i}^{(k)} v_{1,i}^{(k)}$$

$$\dot{v}_{2,i}^{(k)} = \frac{Q_1 (v_{1,i}^{(k)})^2 - k_B T}{Q_2} - \gamma v_{2,i}^{(k)} + \sqrt{\frac{2\gamma}{\beta Q_2}}\eta(t) \qquad k = \overline{1, L} \tag{78}$$

with an isokinetic constraint on each degree of freedom taking the form

$$\frac{p_i^2}{m_i} + \frac{L}{L+1}\sum_{k=1}^{L} (v_{1,i}^{(k)})^2 Q_1 = L k_B T \tag{79}$$

where $k = \overline{1, L}$ labels the thermostat variables, γ is the friction coefficient, Q_1 and Q_2 are thermostat coupling parameters, and λ_i is a Lagrange multiplier for enforcing the isokinetic

DOI: 10.1021/acs.jpca.9b02771
J. Phys. Chem. A 2019, 123, 6056−6079

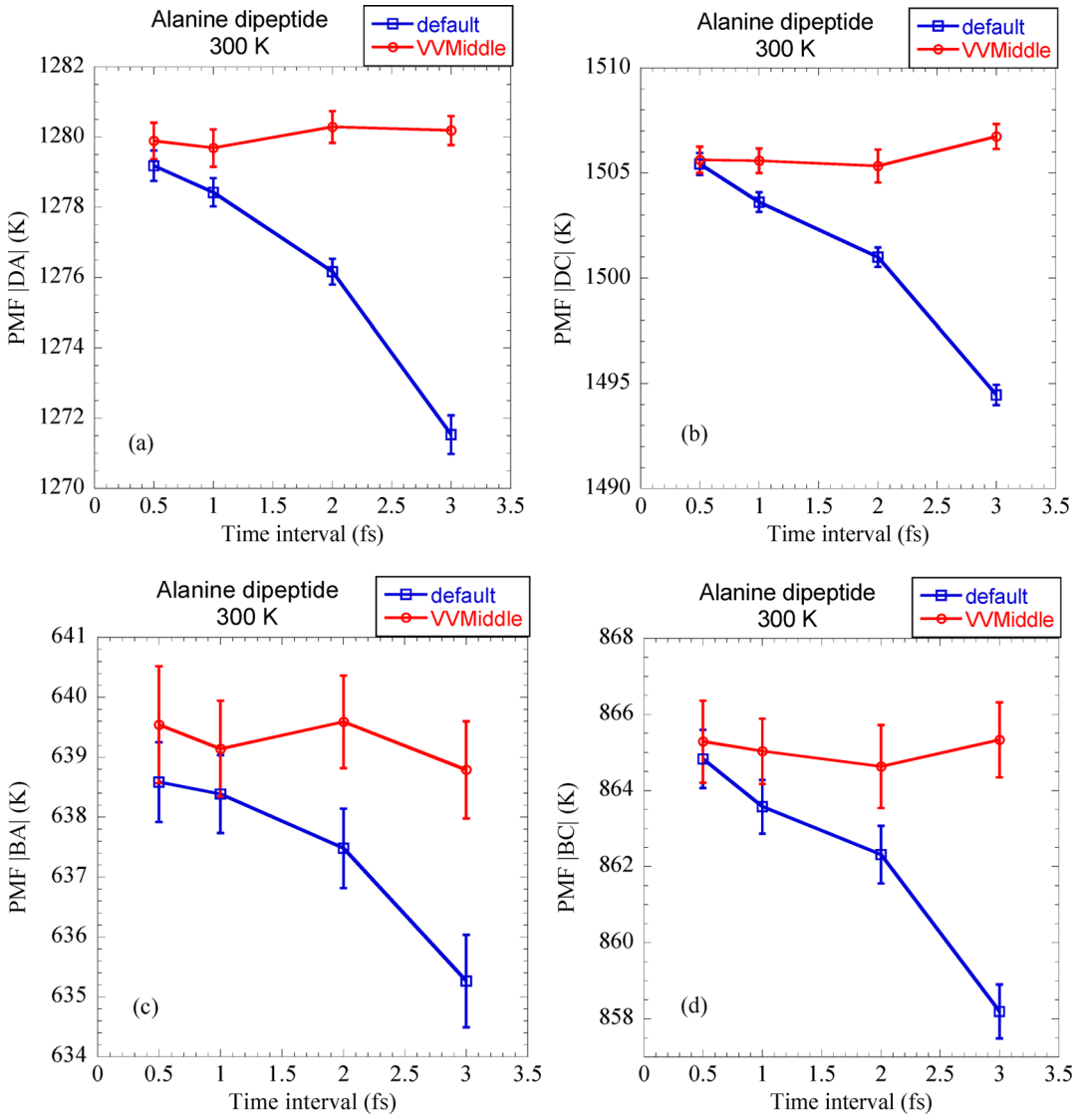

Figure 9. Barriers of the potential of mean force (PMF) for the torsion angle ψ for alanine dipeptide solvated in an implicit solvent model at 300 K (unit: kelvin). (a) |DA| (b) |DC| (c) |BA| (d) |BC|. E.g., |DA| denotes the absolute difference between the PMF of point D and that of point A in Figure 8.

constraint, whose explicit expression can be obtained by differentiating the equation

$$\frac{2p_i\dot{p}_i}{m_i} + \frac{2L}{L+1}\sum_{k=1}^{L} Q_1 v_{1,i}^{(k)} \dot{v}_{1,i}^{(k)} = 0 \tag{80}$$

Substituting the second equation of eq 78 into eq 80 leads to

$$\frac{2p_i}{m_i}\left(-\frac{\partial U}{\partial x_i} - \lambda_i p_i\right) + \frac{2L}{L+1}\sum_{k=1}^{L} Q_1 v_{1,i}^{(k)}\left(-\lambda_i v_{1,i}^{(k)} - v_{2,i}^{(k)} v_{1,i}^{(k)}\right) = 0 \tag{81}$$

which produces the solution for λ_i

$$\lambda_i = -\frac{\frac{p_i}{m_i}\frac{\partial U}{\partial x_i} + \frac{L}{L+1}\sum_{k=1}^{L} Q_1 v_{2,i}^{(k)} (v_{1,i}^{(k)})^2}{\frac{p_i^2}{m_i} + \frac{L}{L+1}\sum_{k=1}^{L} Q_1 (v_{1,i}^{(k)})^2} \tag{82}$$

MTS decomposes the force into a fast component and a slow one

$$\frac{\partial U}{\partial \mathbf{x}} = \frac{\partial U_f}{\partial \mathbf{x}} + \frac{\partial U_s}{\partial \mathbf{x}} \tag{83}$$

Define

$$\lambda_{i,F}^{(f)} = -\frac{\frac{p_i}{m_i}\frac{\partial U_f}{\partial x_i}}{\frac{p_i^2}{m_i} + \frac{L}{L+1}\sum_{k=1}^{L} Q_1 (v_{1,i}^{(k)})^2} \tag{84}$$

$$\lambda_{i,F}^{(s)} = -\frac{\frac{p_i}{m_i}\frac{\partial U_s}{\partial x_i}}{\frac{p_i^2}{m_i} + \frac{L}{L+1}\sum_{k=1}^{L} Q_1 (v_{1,i}^{(k)})^2} \tag{85}$$

and

$$\lambda_{i,N} = -\frac{\frac{L}{L+1}\sum_{k=1}^{L} Q_1 v_{2,i}^{(k)} (v_{1,i}^{(k)})^2}{\frac{p_i^2}{m_i} + \frac{L}{L+1}\sum_{k=1}^{L} Q_1 (v_{1,i}^{(k)})^2} \tag{86}$$

such that $\lambda_i = \lambda_{i,F}^{(f)} + \lambda_{i,F}^{(s)} + \lambda_{i,N}$. From eq 78 we obtain

DOI: 10.1021/acs.jpca.9b02771
J. Phys. Chem. A 2019, 123, 6056−6079

$$\dot{x}_i = \frac{p_i}{m_i}$$

$$\dot{p}_i = -\frac{\partial U}{\partial x_i} - (\lambda_{i,F}^{(f)} + \lambda_{i,F}^{(s)} + \lambda_{i,N})p_i$$

$$\dot{v}_{1,i}^{(k)} = -(\lambda_{i,F}^{(f)} + \lambda_{i,F}^{(s)} + \lambda_{i,N})v_{1,i}^{(k)} - v_{2,i}^{(k)}v_{1,i}^{(k)}$$

$$\dot{v}_{2,i}^{(k)} = \frac{Q_1(v_{1,i}^{(k)})^2 - k_BT}{Q_2} - \gamma v_{2,i}^{(k)} + \sqrt{\frac{2\gamma}{\beta Q_2}}\eta(t) \quad k = \overline{1, L} \tag{87}$$

eq 87 can be recast into 5 parts

$$\begin{pmatrix} \dot{x}_i \\ \dot{p}_i \\ \dot{v}_{1,i}^{(k)} \\ \dot{v}_{2,i}^{(k)} \end{pmatrix} = \underbrace{\begin{pmatrix} \frac{p_i}{m_i} \\ 0 \\ 0 \\ 0 \end{pmatrix}}_{\mathcal{L}_x} + \underbrace{\begin{pmatrix} 0 \\ -\frac{\partial U_f}{\partial x_i} - \lambda_{i,F}^{(f)}p_i \\ -\lambda_{i,F}^{(f)}v_{1,i}^{(k)} \\ 0 \end{pmatrix}}_{\mathcal{L}_p^{(f)}} + \underbrace{\begin{pmatrix} 0 \\ -\frac{\partial U_s}{\partial x_i} - \lambda_{i,F}^{(s)}p_i \\ -\lambda_{i,F}^{(s)}v_{1,i}^{(k)} \\ 0 \end{pmatrix}}_{\mathcal{L}_p^{(s)}}$$
$$+ \underbrace{\begin{pmatrix} 0 \\ -\lambda_{i,N}p_i \\ -\lambda_{i,N}v_{1,i}^{(k)} - v_{2,i}^{(k)}v_{1,i}^{(k)} \\ \frac{Q_1(v_{1,i}^{(k)})^2 - k_BT}{Q_2} \end{pmatrix}}_{\mathcal{L}_N} + \underbrace{\begin{pmatrix} 0 \\ 0 \\ 0 \\ -\gamma v_{2,i}^{(k)} + \sqrt{\frac{2\gamma}{\beta Q_2}}\eta(t) \end{pmatrix}}_{\mathcal{L}_O} \tag{88}$$

The relevant Kolmogorov operators are as follows:

$$\mathcal{L}_x\rho = -\mathbf{p}^T\mathbf{M}^{-1}\frac{\partial\rho}{\partial\mathbf{x}} \tag{89}$$

$$\mathcal{L}_p^{(f)}\rho = \sum_{i=1}^{3N}\left[\left(\frac{\partial U_f}{\partial x_i} + \lambda_{i,F}^{(f)}p_i\right)\frac{\partial\rho}{\partial p_i} + \lambda_{i,F}^{(f)}\sum_{k=1}^{L}v_{1,i}^{(k)}\frac{\partial\rho}{\partial v_{1,i}^{(k)}}\right] \tag{90}$$

$$\mathcal{L}_p^{(s)}\rho = \sum_{i=1}^{3N}\left[\left(\frac{\partial U_s}{\partial x_i} + \lambda_{i,F}^{(s)}p_i\right)\frac{\partial\rho}{\partial p_i} + \lambda_{i,F}^{(s)}\sum_{k=1}^{L}v_{1,i}^{(k)}\frac{\partial\rho}{\partial v_{1,i}^{(k)}}\right] \tag{91}$$

$$\mathcal{L}_N\rho = \sum_{i=1}^{3N}\left[\lambda_{i,N}p_i\frac{\partial\rho}{\partial p_i} + \sum_{k=1}^{L}(\lambda_{i,N}v_{1,i}^{(k)} + v_{2,i}^{(k)}v_{1,i}^{(k)})\frac{\partial\rho}{\partial v_{1,i}^{(k)}} - \sum_{k=1}^{L}\frac{Q_1(v_{1,i}^{(k)})^2 - k_BT}{Q_2}\frac{\partial\rho}{\partial v_{2,i}^{(k)}}\right] \tag{92}$$

$$\mathcal{L}_O\rho = \sum_{i=1}^{3N}\sum_{k=1}^{L}\left[\frac{\partial}{\partial v_{2,i}^{(k)}}(\gamma v_{2,i}^{(k)}\rho) + \frac{\gamma}{\beta Q_2}\frac{\partial^2\rho}{\partial v_{2,i}^{(k)2}}\right] \tag{93}$$

Suppose $\Delta t = n\delta t$, with Δt and δt as the outer and inner time intervals (or steps), respectively. The original version of SIN(R)[49] employs the following propagating order

$$e^{\mathcal{L}\Delta t} \approx e^{\mathcal{L}_N\delta t/2}e^{\mathcal{L}_p^{(f)}\delta t/2 + \mathcal{L}_p^{(s)}\Delta t/2}e^{\mathcal{L}_x\delta t/2}e^{\mathcal{L}_O\delta t}e^{\mathcal{L}_x\delta t/2}e^{\mathcal{L}_p^{(f)}\delta t/2}e^{\mathcal{L}_N\delta t/2}$$
$$\times (e^{\mathcal{L}_N\delta t/2}e^{\mathcal{L}_p^{(f)}\delta t/2}e^{\mathcal{L}_x\delta t/2}e^{\mathcal{L}_O\delta t}e^{\mathcal{L}_x\delta t/2}e^{\mathcal{L}_p^{(f)}\delta t/2}e^{\mathcal{L}_N\delta t/2})^{n-2}$$
$$\times e^{\mathcal{L}_N\delta t/2}e^{\mathcal{L}_p^{(f)}\delta t/2}e^{\mathcal{L}_x\delta t/2}e^{\mathcal{L}_O\delta t}e^{\mathcal{L}_x\delta t/2}e^{\mathcal{L}_p^{(f)}\delta t/2 + \mathcal{L}_p^{(s)}\Delta t/2}e^{\mathcal{L}_N\delta t/2} \tag{94}$$

As we have already pointed out in refs 10,11 on the unified thermostat framework, it is always advantageous to leave the thermostat part(s) in the middle of the whole numerical integration for a time interval to gain efficiency and accuracy in sampling the configurational space. It is then natural for one to apply "VV-Middle" to propose the propagating order

$$e^{\mathcal{L}\Delta t} \approx e^{\mathcal{L}_p^{(f)}\delta t/2 + \mathcal{L}_p^{(s)}\Delta t/2}e^{\mathcal{L}_x\delta t/2}e^{\mathcal{L}_N\delta t/2}e^{\mathcal{L}_O\delta t}e^{\mathcal{L}_N\delta t/2}e^{\mathcal{L}_x\delta t/2}e^{\mathcal{L}_p^{(f)}\delta t/2}$$
$$\times (e^{\mathcal{L}_p^{(f)}\delta t/2}e^{\mathcal{L}_x\delta t/2}e^{\mathcal{L}_N\delta t/2}e^{\mathcal{L}_O\delta t}e^{\mathcal{L}_N\delta t/2}e^{\mathcal{L}_x\delta t/2}e^{\mathcal{L}_p^{(f)}\delta t/2})^{n-2}$$
$$\times e^{\mathcal{L}_p^{(f)}\delta t/2}e^{\mathcal{L}_x\delta t/2}e^{\mathcal{L}_N\delta t/2}e^{\mathcal{L}_O\delta t}e^{\mathcal{L}_N\delta t/2}e^{\mathcal{L}_x\delta t/2}e^{\mathcal{L}_p^{(f)}\delta t/2 + \mathcal{L}_p^{(s)}\Delta t/2} \tag{95}$$

which is denoted "VV-Middle-SIN(R)" throughout the paper. We note that it is also straightforward to implement the leapfrog version of the "middle" scheme ("LF-Middle") to obtain the propagating order

$$e^{\mathcal{L}\Delta t} \approx e^{\mathcal{L}_x\delta t/2}e^{\mathcal{L}_N\delta t/2}e^{\mathcal{L}_O\delta t}e^{\mathcal{L}_N\delta t/2}e^{\mathcal{L}_x\delta t/2}e^{\mathcal{L}_p^{(f)}\delta t}$$
$$\times (e^{\mathcal{L}_x\delta t/2}e^{\mathcal{L}_N\delta t/2}e^{\mathcal{L}_O\delta t}e^{\mathcal{L}_N\delta t/2}e^{\mathcal{L}_x\delta t/2}e^{\mathcal{L}_p^{(f)}\delta t})^{n-2}$$
$$\times e^{\mathcal{L}_x\delta t/2}e^{\mathcal{L}_N\delta t/2}e^{\mathcal{L}_O\delta t}e^{\mathcal{L}_N\delta t/2}e^{\mathcal{L}_x\delta t/2}e^{\mathcal{L}_p^{(f)}\delta t + \mathcal{L}_p^{(s)}\Delta t} \tag{96}$$

which is expected to share the same efficiency and accuracy for configurational sampling as eq 95. Below we focus the discussion on eq 95.

When conventional thermostats, such as the Andersen thermostat, Langevin dynamics, and NHC, are used with MTS in "VV-Middle", the Kolmogorov operators relevant to the evolution are

$$\mathcal{L}_x\rho = -\mathbf{p}^T\mathbf{M}^{-1}\frac{\partial\rho}{\partial\mathbf{x}} \tag{97}$$

$$\mathcal{L}_p^{(f)}\rho = \frac{\partial U_f}{\partial\mathbf{x}}\frac{\partial\rho}{\partial\mathbf{p}} \tag{98}$$

$$\mathcal{L}_p^{(s)}\rho = \frac{\partial U_s}{\partial\mathbf{x}}\frac{\partial\rho}{\partial\mathbf{p}} \tag{99}$$

and $\mathcal{L}_T$ is defined according to the specific thermostat. The propagating order is then

$$e^{\mathcal{L}\Delta t} \approx e^{\mathcal{L}_p^{(s)}\Delta t/2}(e^{\mathcal{L}_p^{(f)}\delta t/2}e^{\mathcal{L}_x\delta t/2}e^{\mathcal{L}_T\delta t}e^{\mathcal{L}_x\delta t/2}e^{\mathcal{L}_p^{(f)}\delta t/2})^n e^{\mathcal{L}_p^{(s)}\Delta t/2} \tag{100}$$

which is denoted "VV-Middle-MTS" throughout the paper.

Finally, we note that these schemes are all easily generalizable to implementation with more than two time steps as was done in ref 49.

5. RESULTS AND DISCUSSION FOR SIN(R)

We use a system of liquid water to run numerical simulations for comparing SIN(R), "VV-Middle-SIN(R)", and "VV-Middle-MTS". We use POLI2VS—a polarizable and flexible force field for liquid water.[63] MD simulations are carried out at the temperature 298.15 K with a liquid density of 0.997 g·cm^{-3} for a system of 216 H_2O molecules in a box with periodic boundary conditions. The charge−charge, charge−dipole, and dipole−dipole interactions are treated by the Ewald summation, while the repulsion−dispersion forces and the electrostatic interactions including quadrupoles are cut off from 9.0 to 9.1 Å with the smoothing function. When SIN(R) and "VV-Middle-SIN(R)" are employed, $L = 4$ sets of thermostat variables are

DOI: 10.1021/acs.jpca.9b02771
J. Phys. Chem. A 2019, 123, 6056−6079

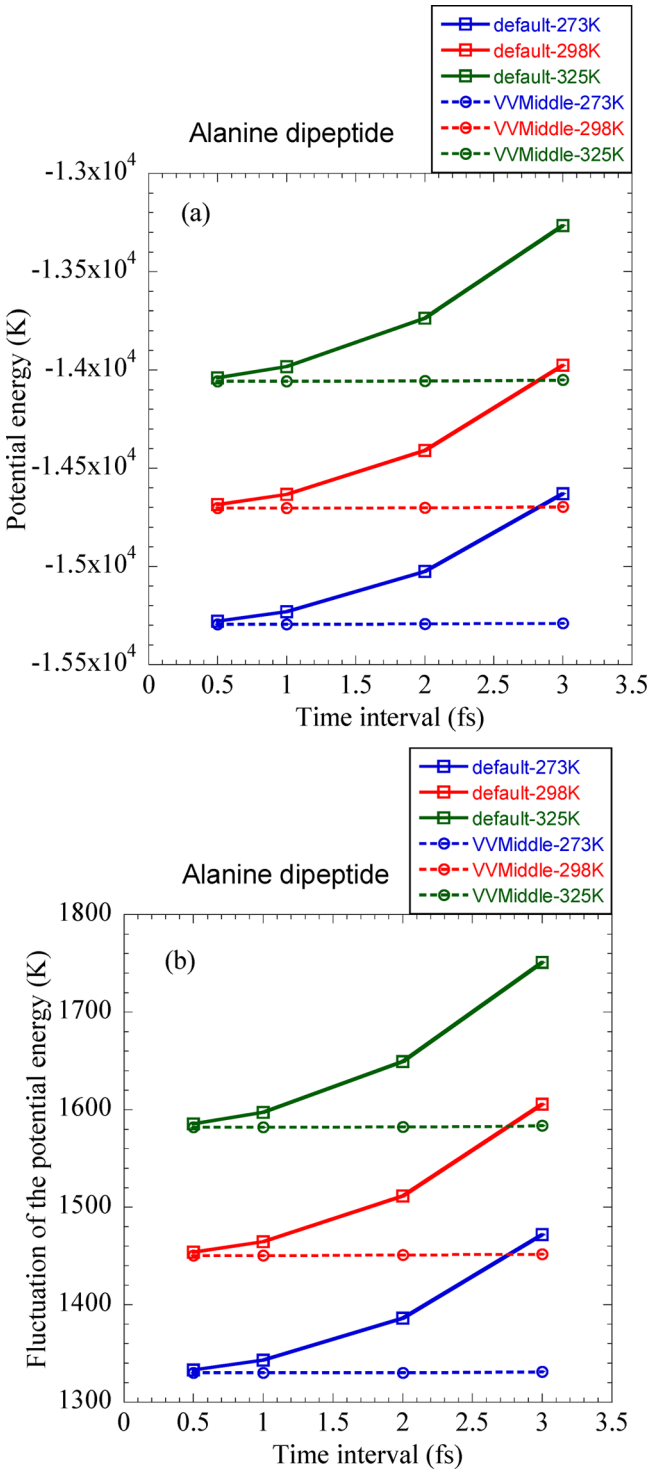

Figure 10. REMD results using different time intervals for alanine dipeptide at different temperatures. (a) averaged potential energy $\langle U(\mathbf{x})\rangle/k_B$ (unit: kelvin) (b) fluctuation of the potential energy $\sqrt{\langle U(\mathbf{x})^2\rangle - \langle U(\mathbf{x})\rangle^2}/k_B$ (unit: kelvin).

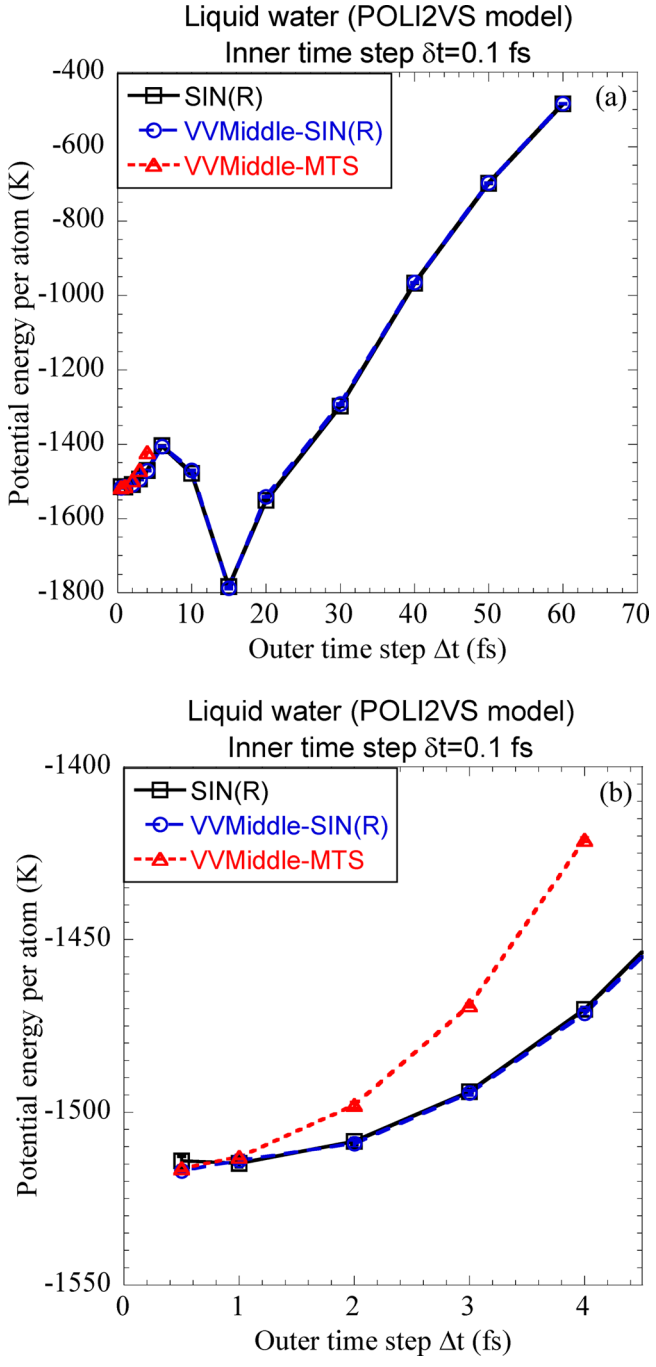

Figure 11. MD results for the average potential energy per atom $\langle U(\mathbf{x})\rangle/(N_{atom}k_B)$ (unit: kelvin) of liquid water at T = 298.15 K as a function of the outer time step Δt when inner time step is fixed at δt = 0.1 fs: (a) Δt in the range 0.5−60 fs and (b) Δt in the range 0.5−4 fs.

coupled to each degree of freedom, the thermostat coupling parameters are chosen as $Q_1 = Q_2 = k_BT(0.01\ \text{ps})^2$ and the friction coefficient is chosen as $\gamma = 5\ \text{ps}^{-1}$. We use $\gamma = 5\ \text{ps}^{-1}$ for Langevin dynamics in "VV-Middle-MTS". After the system approaches the equilibrium, 20 MD trajectories with each propagated up to 100 ps are used for estimating thermodynamic properties. In MTS, the force derived from the intramolecular bonds and angles is treated as the fast component, while the force obtained from the Lennard-Jones and electrostatic interactions is employed as the slow component. Δt and δt represent the outer and inner time steps. For a proof of concept, this simple two time-step scheme is sufficient. It is easy to generalize to cases when three time steps are used, with the middle and outer time step applied to short-range nonbonded and long-range nonbonded interactions as was done in ref 49 to show the type of high performance that is what the SIN(R) algorithm, being a resonance-free MTS algorithm, was designed for. In a future publication, we will demonstrate the

DOI: 10.1021/acs.jpca.9b02771
J. Phys. Chem. A 2019, 123, 6056−6079

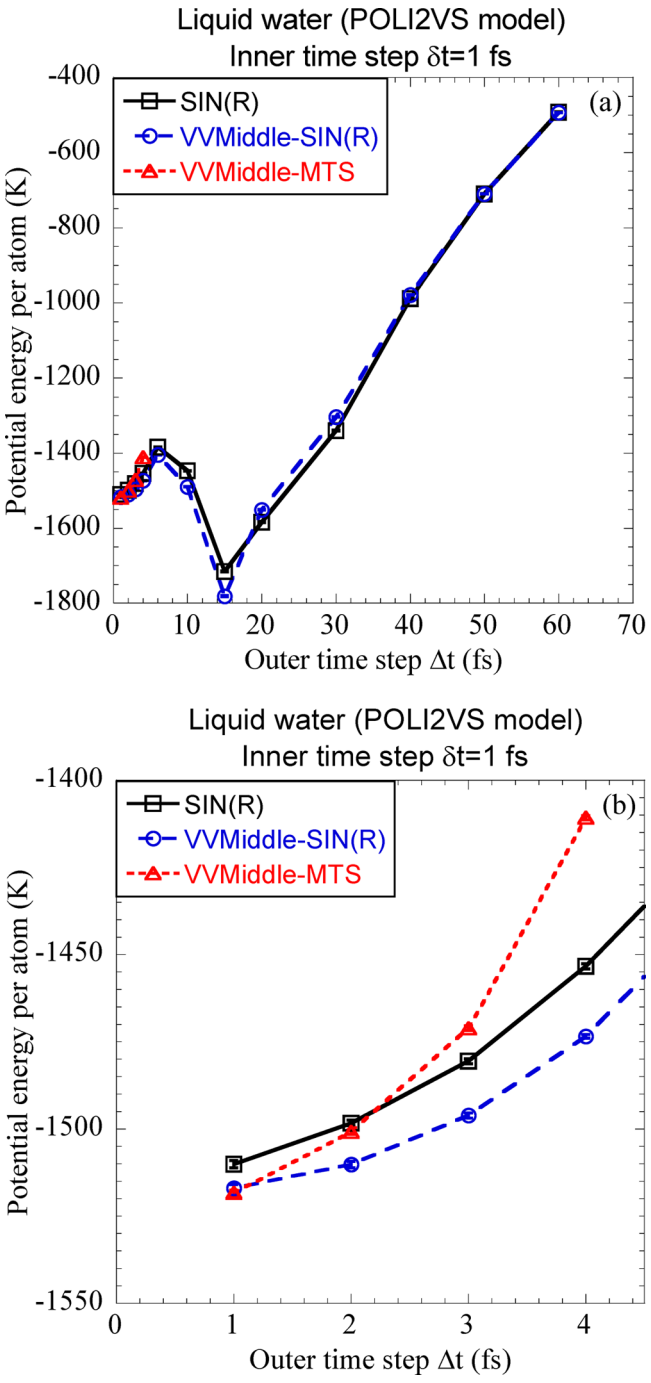

Figure 12. Same as Figure 11, but for the inner time step δt = 1 fs.

performance for MTS decompositions, exploiting the time-scale separation between short- and long-range forces, which allow even larger time steps.

Figure 11 or Figure 12 shows the results when the inner time step is fixed at δt = 0.1 fs or δt = 1 fs but the outer one Δt varies. In this case SIN(R) and "VV-Middle-SIN(R)" perform similarly as the outer time step Δt increases. Figure 13 demonstrates the results when the outer time step Δt is fixed at 1, 2, or 4 fs but the inner one δt changes. Consider the (average) potential energy (per atom) with the outer time step Δt fixed at 2 fs as shown in Figure 13b. "VV-Middle-SIN(R)" and SIN(R) lead to almost the same result for δt = 0.1 fs, which we use as the reference. The largest deviation from this reference produced by "VV-Middle-SIN(R)" is less than 7 K, while that yielded by

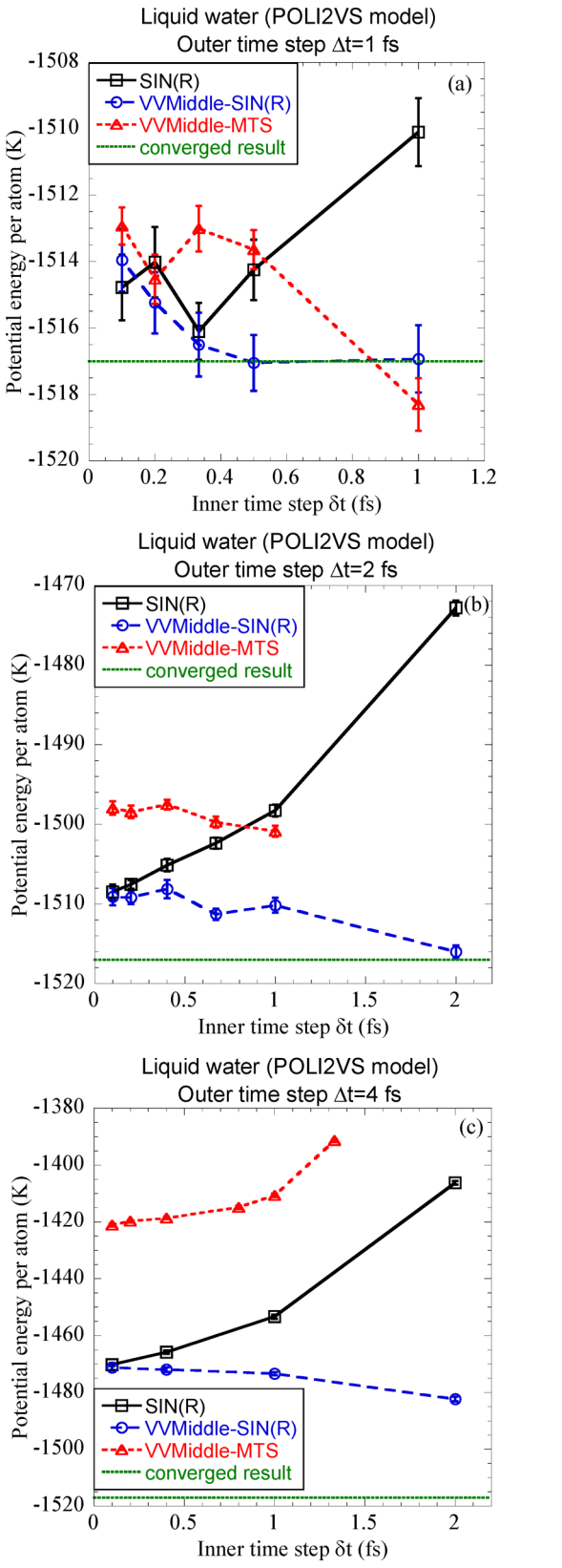

Figure 13. MD results for the average potential energy per atom $\langle U(\mathbf{x})\rangle/(N_{\text{atom}}k_B)$ (unit: kelvin) of liquid water at T = 298.15 K as a function of the inner time step δt while using different fixed values for the outer time step: (a) Δt = 1 fs, (b) Δt = 2 fs, and (c) Δt = 4 fs.

SIN(R) can be more than 35 K. Figure 13c demonstrates that the same property for "VV-Middle-SIN(R)" is less than 11 K and

DOI: 10.1021/acs.jpca.9b02771
J. Phys. Chem. A 2019, 123, 6056−6079

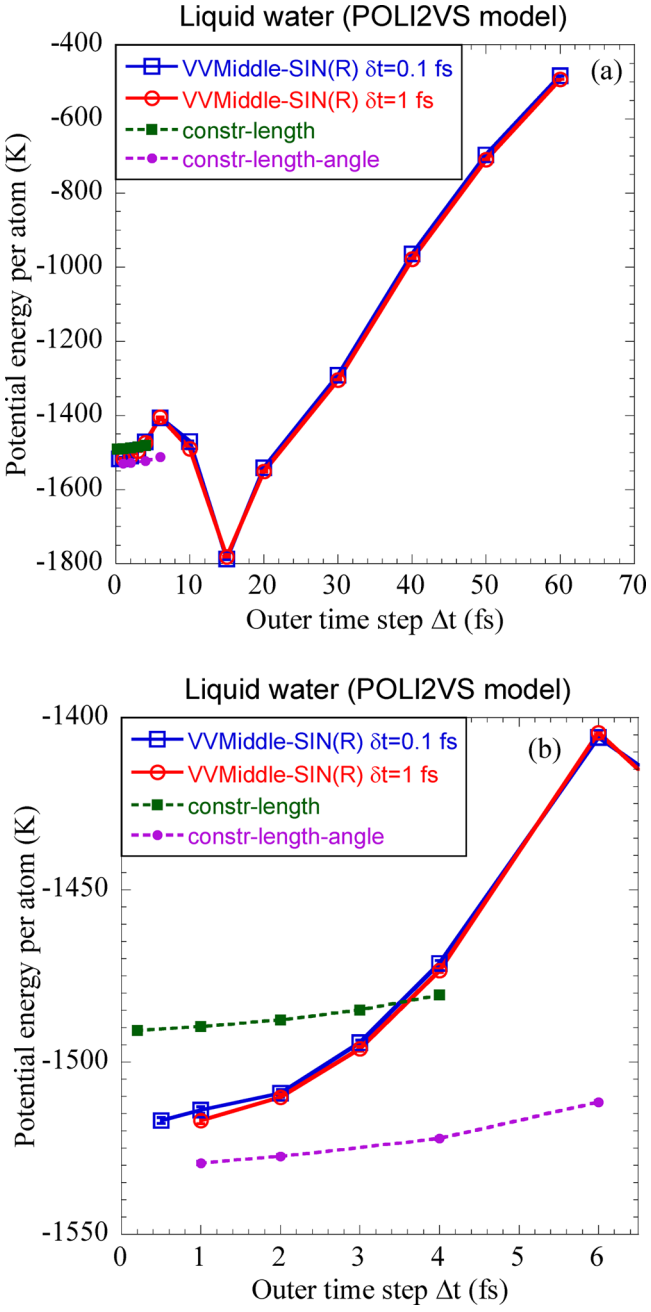

Figure 14. Comparison between the multiple time-step scheme and constrained dynamics. MD results for the average potential energy per atom $\langle U(\mathbf{x})\rangle/(N_{\text{atom}}k_B)$ (unit: kelvin) of liquid water at T = 298.15 K as a function of the time step (outer time step Δt for the multiple time-step scheme). The inner time step δt is fixed at 0.1 or 1 fs for the multiple time-step scheme: (a) Δt in the range 0.2−60 fs and (b) Δt in the range 0.2−6 fs.

that for SIN(R) is more than 64 K. Overall, "VV-Middle-SIN(R)" leads to more stable and accurate results than SIN(R) does as the inner time step increases.

We then use the same system to compare the "VV-Middle-SIN(R)" approach with dynamics with holonomic constraints in the "middle" scheme as described in section 2. In constrained MD simulations with the POLI2VS water force field, the values of two O−H bond lengths of each water molecule are fixed at 0.917 Å when intramolecular O−H bond lengths are constrained, and the value of the H−O−H bond angle in each water molecule is fixed at 104.508° when the intramolecular H−O−H bond angle is frozen. We consider four cases: (1) "VV-Middle-SIN(R)" with the inner time step fixed at δt = 0.1 fs; (2) "VV-Middle-SIN(R)" with the inner time step fixed at δt = 1 fs; (3) step where only (intramolecular) O−H bond lengths are constrained (but the bending motion is allowed); (4) step where both intramolecular O−H bond lengths and H−O−H bond angles are constrained (i.e., intramolecular bending and stretching vibrational motions are frozen). As shown in Figure 14 for the (average) potential (per atom), MD with holonomic constraints in the "middle" scheme (as described in section 2) performs similarly as the time interval (step size) changes and can lead to results that are relatively insensitive to the time interval. In comparison, "VV-Middle-SIN(R)" can employ a much larger (outer) time step without breaking down the propagation of the trajectory if the (lower) accuracy is acceptable.

6. CONCLUSIONS AND OUTLOOK

The "middle" thermostat scheme[8,10,11,34,35] is a promising approach for constructing novel efficient MD algorithms for configurational sampling for systems subject to constraints. We use two types of constraints, namely, holonomic constraints and isokinetic constraints, for demonstration. Numerical simulations suggest that the thermostat algorithms within the "middle" scheme are superior to conventional ones in sampling the marginal distribution of the configuration, leading to more accurate results for configuration-dependent thermodynamic properties when the same finite time interval Δt is used. Employing the "middle" scheme with resonance-free multiple time-step techniques also produces more efficient and accurate algorithms for configurational sampling for the systems treated via multiple time stepping with just two time steps. It is easy to extend the strategy to cases when three or more time steps are employed, as we will be demonstrating in a future publication.

In addition to constraints and multiple time-step methods, it is straightforward to implement the "middle" thermostat scheme (for MD as well as PIMD) together with various advanced enhanced sampling techniques[71,74−80] (e.g., replica exchange[71] as we have used in this paper, integrated tempering sampling,[77] meta-dynamics,[75,78] blue moon,[81−83] milestoning,[84] etc.) to accelerate configurational sampling for systems involving rare events. Because the "middle" thermostat scheme in principle takes no advantage of the specific form of the force or potential energy surface, it will be useful to implement the "middle" scheme for ab initio MD (or ab initio PIMD).[70,85] It is important to note that all strategies introduced for the "middle" scheme for MD in the paper are straightforward to implement for PIMD (subject to various constraints or with resonance-free multiple time-step techniques). Some of them have already been employed for PIMD simulations of liquid water with holonomic constraints.[86] We expect that the results in this paper as well as those in a series of papers[8,10,11,34,35] and the implementation in AMBER[67] will encourage others to use the "middle" scheme to develop various efficient MD (and PIMD) algorithms or do simulations for configurational sampling for systems of their interest.

In future work, it will be interesting to use the "middle" scheme[8,10,11,34,35] in the rational design of yet more efficient algorithms (with resonance-free multiple time-step techniques as well as constraint approaches), particularly for use with other constant temperature ensembles beyond the canonical (NVT) ensemble, e.g., the isothermal−isobaric (NPT) ensemble.

DOI: 10.1021/acs.jpca.9b02771
J. Phys. Chem. A 2019, 123, 6056−6079

■ ASSOCIATED CONTENT

Supporting Information

The Supporting Information is available free of charge on the ACS Publications website at DOI: 10.1021/acs.jpca.9b02771.

Another viewpoint for the "middle" scheme subject to holonomic constraints, analytical analysis for harmonic system subject to linear constraints, additional numerical tests for constrained MD algorithms, pseudo code for SIN(R) in the velocity−Verlet "middle" scheme, and parameters for SIN(R) (PDF)

■ AUTHOR INFORMATION

Corresponding Author

*(J.L.) E-mail: jianliupku@pku.edu.cn.

ORCID

Mark E. Tuckerman: 0000-0003-2194-9955

Jian Liu: 0000-0002-2906-5858

Author Contributions

⊥Both authors contributed equally to the work.

Notes

The authors declare no competing financial interest.

Biography

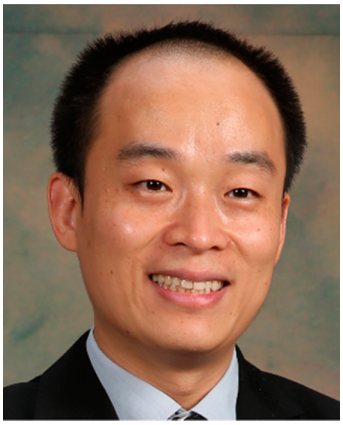

Jian Liu received his Ph.D. in Physical Chemistry in 2005 from the University of Illinois at Urbana−Champaign. He then spent a postdoc at the University of California, Berkeley, and was a research associate at Stanford University before he joined Peking University as an Associate Professor in December 2012. His research interest has focused on the development of theories and methodologies of quantum/semiclassical dynamics and quantum/classical statistics for complex (large) molecular systems.

■ ACKNOWLEDGMENTS

This work was supported by the Ministry of Science and Technology of China (MOST) Grant no. 2016YFC0202803 and no. 2017YFA0204901, by the National Natural Science Foundation of China (NSFC) Grant no. 21373018 and no. 21573007, by the Recruitment Program of Global Experts, by Specialized Research Fund for the Doctoral Program of Higher Education no. 20130001110009, and by the Special Program for Applied Research on Super Computation of the NSFC-Guangdong Joint Fund (the second phase) under Grant no. U1501501. M.E.T. acknowledges funding from the US National Science Foundation grant no. CHE-1565980. We acknowledge the Beijing and Tianjin supercomputer centers and the High-performance Computing Platform of Peking University for providing computational resources.

■ REFERENCES

(1) Fermi, E.; Pasta, J. R.; Ulam, S.; Tsingou, M Studies of Nonlinear Problems. *Los Alamos Report* **1955**, LA-1940.

(2) Alder, B. J.; Wainwright, T. E. Phase Transition for a Hard Sphere System. *J. Chem. Phys.* **1957**, *27*, 1208−1209.

(3) Allen, M. P.; Tildesley, D. J. *Computer Simulation of Liquids*; Clarendon Press: 1989.

(4) Frenkel, D.; Smit, B. *Understanding Molecular Simulation*, 2nd ed.; ; Academic Press: San Diego, CA, 2002.

(5) Parrinello, M.; Rahman, A. Study of an F Center in Molten KCl. *J. Chem. Phys.* **1984**, *80*, 860−867.

(6) Berne, B. J.; Thirumalai, D. On the Simulation of Quantum Systems: Path Integral Methods. *Annu. Rev. Phys. Chem.* **1986**, *37*, 401−424.

(7) Tuckerman, M. E. *Statistical Mechanics: Theory and Molecular Simulation*; Oxford University Press: New York, 2010.

(8) Liu, J.; Li, D.; Liu, X. A Simple and Accurate Algorithm for Path Integral Molecular Dynamics with the Langevin Thermostat. *J. Chem. Phys.* **2016**, *145*, 024103.

(9) Markland, T. E.; Ceriotti, M. Nuclear Quantum Effects Enter the Mainstream. *Nat. Rev. Chem.* **2018**, *2*, 0109.

(10) Zhang, Z.; Liu, X.; Chen, Z.; Zheng, H.; Yan, K.; Liu, J. A Unified Thermostat Scheme for Efficient Configurational Sampling for Classical/Quantum Canonical Ensembles via Molecular Dynamics. *J. Chem. Phys.* **2017**, *147*, 034109.

(11) Zhang, Z.; Yan, K.; Liu, X.; Liu, J. A Leap-Frog Algorithm-Based Efficient Unified Thermostat Scheme for Molecular Dynamics. *Chin. Sci. Bull.* **2018**, *63*, 3467.

(12) Andersen, H. C. Molecular Dynamics Simulations at Constant Pressure and/or Temperature. *J. Chem. Phys.* **1980**, *72*, 2384−2393.

(13) Nosé, S. A Molecular Dynamics Method for Simulations in the Canonical Ensemble. *Mol. Phys.* **1984**, *52*, 255−268.

(14) Hoover, W. G. Canonical Dynamics: Equilibrium Phase-Space Distributions. *Phys. Rev. A: At., Mol., Opt. Phys.* **1985**, *31*, 1695−1697.

(15) Martyna, G. J.; Klein, M. L.; Tuckerman, M. Nosé−Hoover Chains: The Canonical Ensemble via Continuous Dynamics. *J. Chem. Phys.* **1992**, *97*, 2635−2643.

(16) Martyna, G. J.; Tuckerman, M. E.; Tobias, D. J.; Klein, M. L. Explicit Reversible Integrators for Extended Systems Dynamics. *Mol. Phys.* **1996**, *87*, 1117−1157.

(17) Tuckerman, M.; Berne, B. J.; Martyna, G. J. Reversible Multiple Time Scale Molecular Dynamics. *J. Chem. Phys.* **1992**, *97*, 1990−2001.

(18) Andrea, T. A.; Swope, W. C.; Andersen, H. C. The Role of Long Ranged Forces in Determining the Structure and Properties of Liquid Water. *J. Chem. Phys.* **1983**, *79*, 4576−4584.

(19) Brünger, A.; Brooks, C. L., III; Karplus, M. Stochastic Boundary Conditions for Molecular Dynamics Simulations of ST2 Water. *Chem. Phys. Lett.* **1984**, *105*, 495−500.

(20) Goga, N.; Rzepiela, A. J.; de Vries, A. H.; Marrink, S. J.; Berendsen, H. J. C. Efficient Algorithms for Langevin and DPD Dynamics. *J. Chem. Theory Comput.* **2012**, *8*, 3637−3649.

(21) Bussi, G.; Parrinello, M. Accurate Sampling Using Langevin Dynamics. *Phys. Rev. E* **2007**, *75*, 056707.

(22) Grønbech-Jensen, N.; Farago, O. A Simple and Effective Verlet-Type Algorithm for Simulating Langevin Dynamics. *Mol. Phys.* **2013**, *111*, 983−991.

(23) Leimkuhler, B.; Matthews, C. Rational Construction of Stochastic Numerical Methods for Molecular Sampling. *Appl. Math. Res. Express* **2012**, *2013*, 34−56.

(24) Leimkuhler, B.; Matthews, C. Robust and Efficient Configurational Molecular Sampling via Langevin Dynamics. *J. Chem. Phys.* **2013**, *138*, 174102.

(25) Leimkuhler, B.; Matthews, C. Efficient Molecular Dynamics Using Geodesic Integration and Solvent−Solute Splitting. *Proc. R. Soc. London, Ser. A* **2016**, *472*, 20160138.

(26) Leimkuhler, B.; Matthews, C. *Molecular Dynamics With Deterministic and Stochastic Numerical Methods*; Springer: 2015.

(27) Hall, R.; Berne, B. J. Nonergodicity in Path Integral Molecular Dynamics. *J. Chem. Phys.* **1984**, *81*, 3641−3643.

DOI: 10.1021/acs.jpca.9b02771
J. Phys. Chem. A 2019, 123, 6056−6079

(28) Gillan, M. J. Quantum Simulation of Hydrogen in Metals. *Phys. Rev. Lett.* **1987**, *58*, 563−566.
(29) Singer, K.; Smith, W. Path Integral Simulations of Condensed Phase Lennard-Jones Systems. *Mol. Phys.* **1988**, *64*, 1215−1231.
(30) Müser, M. H. On New Efficient Algorithms for PIMC and PIMD. *Comput. Phys. Commun.* **2002**, *147*, 83−86.
(31) Drozdov, A. N.; Talkner, P. Path Integrals for Fokker-Planck Dynamics with Singular Diffusion: Accurate Factorization for the Time Evolution Operator. *J. Chem. Phys.* **1998**, *109*, 2080−2091.
(32) Tuckerman, M. E.; Marx, D.; Klein, M. L.; Parrinello, M. Efficient and General Algorithms for Path Integral Car-Parrinello Molecular Dynamics. *J. Chem. Phys.* **1996**, *104*, 5579−5588.
(33) Ceriotti, M.; Parrinello, M.; Markland, T. E.; Manolopoulos, D. E. Efficient Stochastic Thermostatting of Path Integral Molecular Dynamics. *J. Chem. Phys.* **2010**, *133*, 124104.
(34) Li, D.; Han, X.; Chai, Y.; Wang, C.; Zhang, Z.; Chen, Z.; Liu, J.; Shao, J. Stationary State Distribution and Efficiency Analysis of the Langevin Equation via Real or Virtual Dynamics. *J. Chem. Phys.* **2017**, *147*, 184104.
(35) Li, D.-z.; Chen, Z.-f.; Zhang, Z.-j.; Liu, J. Understanding Molecular Dynamics with Stochastic Processes via Real or Virtual Dynamics. *Chin. J. Chem. Phys.* **2017**, *30*, 735−760.
(36) Ryckaert, J.-P.; Ciccotti, G.; Berendsen, H. J. C. Numerical Integration of the Cartesian Equations of Motion of a System with Constraints: Molecular Dynamics of n-Alkanes. *J. Comput. Phys.* **1977**, *23*, 327−341.
(37) Andersen, H. C. Rattle: A "Velocity" Version of the Shake Algorithm for Molecular Dynamics Calculations. *J. Comput. Phys.* **1983**, *52*, 24−34.
(38) Miyamoto, S.; Kollman, P. A. SETTLE: An Analytical Version of the SHAKE and RATTLE Algorithm for Rigid Water Models. *J. Comput. Chem.* **1992**, *13*, 952−962.
(39) Kräutler, V.; van Gunsteren, W. F.; Hünenberger, P. H. A Fast SHAKE Algorithm to Solve Distance Constraint Equations for Small Molecules in Molecular Dynamics Simulations. *J. Comput. Chem.* **2001**, *22*, 501−508.
(40) Tao, P.; Wu, X.; Brooks, B. R. Maintain Rigid Structures in Verlet Based Cartesian Molecular Dynamics Simulations. *J. Chem. Phys.* **2012**, *137*, 134110.
(41) Hess, B.; Bekker, H.; Berendsen, H. J. C.; Fraaije, J. G. E. M. LINCS: A Linear Constraint Solver for Molecular Simulations. *J. Comput. Chem.* **1997**, *18*, 1463−1472.
(42) Hoover, W. G.; Ladd, A. J. C.; Moran, B. High-Strain-Rate Plastic Flow Studied via Nonequilibrium Molecular Dynamics. *Phys. Rev. Lett.* **1982**, *48*, 1818−1820.
(43) Evans, D. J.; Morriss, G. P. Isothermal-Isobaric Molecular Dynamics. *Chem. Phys.* **1983**, *77*, 63−66.
(44) Evans, D. J.; Morriss, O. P. Non-Newtonian Molecular Dynamics. *Comput. Phys. Rep.* **1984**, *1*, 297−343.
(45) Tuckerman, M. E.; Liu, Y.; Ciccotti, G.; Martyna, G. J. Non-Hamiltonian Molecular Dynamics: Generalizing Hamiltonian Phase Space Principles to Non-Hamiltonian Systems. *J. Chem. Phys.* **2001**, *115*, 1678−1702.
(46) Minary, P.; Martyna, G. J.; Tuckerman, M. E. Algorithms and Novel Applications Based on the Isokinetic Ensemble. I. Biophysical and Path Integral Molecular Dynamics. *J. Chem. Phys.* **2003**, *118*, 2510−2526.
(47) Minary, P.; Tuckerman, M. E.; Martyna, G. J. Long Time Molecular Dynamics for Enhanced Conformational Sampling in Biomolecular Systems. *Phys. Rev. Lett.* **2004**, *93*, 150201.
(48) Omelyan, I.; Kovalenko, A. Generalised Canonical−Isokinetic Ensemble: Speeding up Multiscale Molecular Dynamics and Coupling with 3D Molecular Theory of Solvation. *Mol. Simul.* **2013**, *39*, 25−48.
(49) Leimkuhler, B.; Margul, D. T.; Tuckerman, M. E. Stochastic, Resonance-Free Multiple Time-Step Algorithm for Molecular Dynamics with Very Large Time Steps. *Mol. Phys.* **2013**, *111*, 3579−3594.
(50) Lippert, R. A.; Bowers, K. J.; Dror, R. O.; Eastwood, M. P.; Gregersen, B. A.; Klepeis, J. L.; Kolossvary, I.; Shaw, D. E. A Common, Avoidable Source of Error in Molecular Dynamics Integrators. *J. Chem. Phys.* **2007**, *126*, 046101.
(51) Leimkuhler, B. J.; Skeel, R. D. Symplectic Numerical Integrators in Constrained Hamiltonian Systems. *J. Comput. Phys.* **1994**, *112*, 117−125.
(52) Kalibaeva, G.; Ferrario, M.; Ciccotti, G. Constant Pressure-Constant Temperature Molecular Dynamics: A Correct Constrained NPT Ensemble Using the Molecular Virial. *Mol. Phys.* **2003**, *101*, 765−778.
(53) Toxvaerd, S.; Heilmann, O. J.; Ingebrigtsen, T.; Schrøder, T. B.; Dyre, J. C. Time-Reversible Molecular Dynamics Algorithms with Bond Constraints. *J. Chem. Phys.* **2009**, *131*, 064102.
(54) Toxvaerd, S. Algorithms for Canonical Molecular Dynamics Simulations. *Mol. Phys.* **1991**, *72*, 159−168.
(55) Lelièvre, T.; Rousset, M.; Stoltz, G. Langevin Dynamics with Constraints and Computation of Free Energy Differences. *Math. Comp.* **2012**, *81*, 2071−2215.
(56) Ryckaert, J. P.; Ciccotti, G. Andersen's Canonical-Ensemble Molecular Dynamics for Molecules with Constraints. *Mol. Phys.* **1986**, *58*, 1125−1136.
(57) Peters, E. A. J. F.; Goga, N.; Berendsen, H. J. C. Stochastic Dynamics with Correct Sampling for Constrained Systems. *J. Chem. Theory Comput.* **2014**, *10*, 4208−4220.
(58) Tobias, D. J.; Martyna, G. J.; Klein, M. L. Molecular Dynamics Simulations of a Protein in the Canonical Ensemble. *J. Phys. Chem.* **1993**, *97*, 12959−12966.
(59) Tuckerman, M. E.; Berne, B. J.; Rossi, A. Molecular Dynamics Algorithm for Multiple Time Scales: Systems with Disparate Masses. *J. Chem. Phys.* **1991**, *94*, 1465−1469.
(60) Suzuki, M. Decomposition Formulas of Exponential Operators and Lie Exponentials with Some Applications to Quantum Mechanics and Statistical Physics. *J. Math. Phys.* **1985**, *26*, 601−612.
(61) Yoshida, H. Construction of Higher Order Symplectic Integrators. *Phys. Lett. A* **1990**, *150*, 262−268.
(62) Suzuki, M. General Theory of Fractal Path Integrals with Applications to Many-Body Theories and Statistical Physics. *J. Math. Phys.* **1991**, *32*, 400−407.
(63) Hasegawa, T.; Tanimura, Y. A Polarizable Water Model for Intramolecular and Intermolecular Vibrational Spectroscopies. *J. Phys. Chem. B* **2011**, *115*, 5545−5553.
(64) Partridge, H.; Schwenke, D. W. The Determination of an Accurate Isotope Dependent Potential Energy Surface for Water from Extensive Ab Initio Calculations and Experimental Data. *J. Chem. Phys.* **1997**, *106*, 4618−4639.
(65) Pastor, R. W.; Brooks, B. R.; Szabo, A. An Analysis of the Accuracy of Langevin and Molecular Dynamics Algorithms. *Mol. Phys.* **1988**, *65*, 1409−1419.
(66) Paesani, F.; Zhang, W.; Case, D. A.; Cheatham, T. E.; Voth, G. A. An Accurate and Simple Quantum Model for Liquid Water. *J. Chem. Phys.* **2006**, *125*, 184507.
(67) Case, D. A.; Ben-Shalom, I. Y.; Brozell, S. R.; Cerutti, D. S.; Cheatham, T. E., III; Cruzeiro, V. W. D.; Darden, T. A.; Duke, R. E.; Ghoreishi, D.; Gilson, M. K.; Gohlke, H.; Goetz, A. W.; Greene, D.; Harris, R.; Homeyer, N.; Izadi, S.; Kovalenko, A.; Kurtzman, T.; Lee, T. S.; LeGrand, S.; Li, P.; Lin, C.; Liu, J.; Luchko, T.; Luo, R.; Mermelstein, D. J.; Merz, K. M.; Miao, Y.; Monard, G.; Nguyen, C.; Nguyen, H.; Omelyan, I.; Onufriev, A.; Pan, F.; Qi, R.; Roe, D. R.; Roitberg, A.; Sagui, C.; Schott-Verdugo, S.; Shen, J.; Simmerling, C. L.; Smith, J.; Salomon-Ferrer, R.; Swails, J.; Walker, R. C.; Wang, J.; Wei, H.; Wolf, R. M.; Wu, X.; Xiao, L.; York, D. M.; Kollman, P. A. *AMBER 2018*; University of California: San Francisco, 2018.
(68) Still, W. C.; Tempczyk, A.; Hawley, R. C.; Hendrickson, T. Semianalytical Treatment of Solvation for Molecular Mechanics and Dynamics. *J. Am. Chem. Soc.* **1990**, *112*, 6127−6129.
(69) Onufriev, A.; Bashford, D.; Case, D. A. Modification of the Generalized Born Model Suitable for Macromolecules. *J. Phys. Chem. B* **2000**, *104*, 3712−3720.
(70) Anandakrishnan, R.; Drozdetski, A.; Walker, R. C.; Onufriev, A. V. Speed of Conformational Change: Comparing Explicit and Implicit

DOI: 10.1021/acs.jpca.9b02771
J. Phys. Chem. A 2019, 123, 6056−6079

Solvent Molecular Dynamics Simulations. *Biophys. J.* **2015**, *108*, 1153−1164.
(71) Sugita, Y.; Okamoto, Y. Replica-Exchange Molecular Dynamics Method for Protein Folding. *Chem. Phys. Lett.* **1999**, *314*, 141−151.
(72) Chodera, J. D.; Swope, W. C.; Pitera, J. W.; Seok, C.; Dill, K. A. Use of the Weighted Histogram Analysis Method for the Analysis of Simulated and Parallel Tempering Simulations. *J. Chem. Theory Comput.* **2007**, *3*, 26−41.
(73) Leimkuhler, B.; Noorizadeh, E.; Theil, F. A Gentle Stochastic Thermostat for Molecular Dynamics. *J. Stat. Phys.* **2009**, *135*, 261−277.
(74) Torrie, G. M.; Valleau, J. P. Nonphysical Sampling Distributions in Monte Carlo Free-Energy Estimation: Umbrella Sampling. *J. Comput. Phys.* **1977**, *23*, 187−199.
(75) Laio, A.; Parrinello, M. Escaping Free-Energy Minima. *Proc. Natl. Acad. Sci. U. S. A.* **2002**, *99*, 12562.
(76) Hamelberg, D.; Mongan, J.; McCammon, J. A. Accelerated Molecular Dynamics: A Promising and Efficient Simulation Method for Biomolecules. *J. Chem. Phys.* **2004**, *120*, 11919−11929.
(77) Gao, Y. Q. An Integrate-over-Temperature Approach for Enhanced Sampling. *J. Chem. Phys.* **2008**, *128*, 064105.
(78) Valsson, O.; Parrinello, M. Variational Approach to Enhanced Sampling and Free Energy Calculations. *Phys. Rev. Lett.* **2014**, *113*, 090601.
(79) Valsson, O.; Tiwary, P.; Parrinello, M. Enhancing Important Fluctuations: Rare Events and Metadynamics from a Conceptual Viewpoint. *Annu. Rev. Phys. Chem.* **2016**, *67*, 159−184.
(80) Peters, B. *Reaction Rate Theory and Rare Events Simulations*; Elsevier: Amsterdam, The Netherlands, 2017.
(81) Carter, E. A.; Ciccotti, G.; Hynes, J. T.; Kapral, R. Constrained Reaction Coordinate Dynamics for the Simulation of Rare Events. *Chem. Phys. Lett.* **1989**, *156*, 472−477.
(82) Sprik, M.; Ciccotti, G. Free Energy from Constrained Molecular Dynamics. *J. Chem. Phys.* **1998**, *109*, 7737−7744.
(83) Sergi, A.; Ciccotti, G.; Falconi, M.; Desideri, A.; Ferrario, M. Effective Binding Force Calculation in a Dimeric Protein by Molecular Dynamics Simulation. *J. Chem. Phys.* **2002**, *116*, 6329−6338.
(84) Bello-Rivas, J. M.; Elber, R. Exact Milestoning. *J. Chem. Phys.* **2015**, *142*, 094102.
(85) According to our private communication with Dr. Jingjing Zheng in 2019, the "middle" scheme (for MD and PIMD) has been implemented in the Gaussian development code.
(86) Liu, X.; Liu, J. Critical Role of Quantum Dynamical Effects in the Raman Spectroscopy of Liquid Water. *Mol. Phys.* **2018**, *116*, 755−779.
(87) Tuckerman, M. E.; Berne, B. J.; Martyna, G. J.; Klein, M. L. Efficient Molecular Dynamics and Hybrid Monte Carlo Algorithms for Path Integrals. *J. Chem. Phys.* **1993**, *99*, 2769−2808.

DOI: 10.1021/acs.jpca.9b02771
J. Phys. Chem. A 2019, 123, 6056−6079